Targeted cortical stimulation reveals principles of cortical contextual interactions

Shen Wang[1,2], **Agostina Palmigiano**[4], **Kenneth D. Miller**[4,5], **Stephen D. Van Hooser**[1,2,3]

***For correspondence:**
vanhoosr@brandeis.edu (SVH)

[1]Department of Biology; [2]Volen Center for Complex Systems; [3]Sloan-Swartz Center for Theoretical Neurobiology Brandeis University, Waltham, MA, USA; [4]Center for Theoretical Neuroscience, Columbia University, New York, NY, USA; [5]Dept. of Neuroscience, Swartz Program in Theoretical Neuroscience, Kavli Institute for Brain Science, College of Physicians and Surgeons and Mortimer B. Zuckerman Mind Brain Behavior Institute at Columbia University, New York, NY, USA

Number of Pages: 18

Number of Figures and Tables: 8 Figures, 0 Tables

Number of words: Abstract: 250 words, Intro: 659, Discussion: 1488

Conflicts of interest: The authors declare no competing interests.

Acknowledgements: This work was funded by NIH EY029999 (KDM + SDV), NSF 1707398 (KDM + AP), Gatsby Charitable Foundation GAT3708 (KDM + AP), and Swartz Foundation (AP). We thank members of Miller lab and Van Hooser lab for comments on the work. We thank David Fitzpatrick's lab for providing AAV9-mDlx-ChR2-mCherry-Fishell-3.

Contributions: KDM and SDV designed experiments; SW designed ProjectorScope 2.0 and carried out experiments, modeling, and analysis; AP provided models and interpretations. SW and SDV wrote the paper with input from AP and KDM.

Keywords: inhibition-stabilized networks, thalamocortical, recurrent connections, striate cortex, area 17

Corresponding Author:
Stephen D. Van Hooser,
Brandeis University
415 South St. MS008, Waltham
MA 02453 USA
e-mail: vanhoosr@brandeis.edu

Abstract

Cross-orientation suppression is a classic form of contextual normalization in visual cortex, yet the degree to which cortical circuits participate in the normalization computation is unclear. We visualized orientation maps of individual ferrets, and provided patterned optogenetic stimulation to both excitatory and inhibitory cells in orientation columns that either matched or were orthogonal to the preferred visual orientation of neurons recorded with electrodes. When visual or optogenetic stimulation of columns preferring one orientation was combined with optogenetic stimulation of columns preferring the orthogonal orientation, we observed less suppression than when orthogonal stimulation was provided visually, suggesting that cortical circuits do not provide a large fraction of visual cross-orientation suppression. Integration of visual and optogenetic signals was linear when neurons exhibited low firing rates and became sublinear when neurons exhibited higher firing rates. We probed the nature of sublinearities in cortex by examining the influence of optogenetic stimulation of cortical interneurons. We observed a range of responses, including evidence for paradoxical responses in which interneuron stimulation caused a decrease in inhibitory firing rate, presumably due to the withdrawal of recurrent excitation. These results are compatible with cortical circuits that exhibit strong recurrent excitation with stabilizing inhibition that provides normalization, albeit normalization that is too weak across columns to account for cross-orientation suppression.

Introduction

Responses of neural circuits depend on context. In visual cortex, neurons respond to bars or gratings of a preferred orientation but are also highly influenced by the simultaneous presentation of additional stimuli, such as gratings that are orthogonal to the preferred orientation or flanking stimuli (Bishop et al., 1973; Morrone et al., 1982; Bonds, 1989; DeAngelis et al., 1992; Das and Gilbert, 1999; Cavanaugh et al., 2002; Smith et al., 2006; Busse et al., 2009; MacEvoy et al., 2009). Many of these contextual influences are well-described phenomenologically by a normalization equation that consists of summation and division (Bonds, 1989; Carandini and Heeger, 2011). However, the cortical circuit mechanisms that underlie contextual processing are incompletely understood.

A classic form of normalization is cross-orientation suppression: the response of visual cortical neurons to a preferred orientation is suppressed when an orthogonal stimulus is also presented, even if the neuron exhibits no response to the orthogonal stimulus when presented alone. Understandably, cross-orientation inhibition emerged as an early hypothesis for the circuit implementation of cross-orientation suppression (DeAngelis et al., 1992; Heeger, 1992), but experiments that blocked cortical inhibition or measured the orientation dependence of cortical inhibition did not find evidence consistent with this hypothesis (Anderson et al., 2000; Katzner et al., 2011). Subsequently, careful consideration of the responses of the feed-forward inputs from the lateral geniculate nucleus (LGN) led to a feed-forward hypothesis: that desynchronization of the temporal response phases of the LGN inputs to a given V1 cell, LGN saturation and rectification, and V1 spike threshold could account, in large part, for the reduced responses observed in cross-orientation suppression (Freeman et al., 2002; Li et al., 2006; Priebe and Ferster, 2006; Priebe, 2016). However, experiments using dichoptic presentation of the two gratings showed a weak cortical component of cross-orientation suppression (Sengpiel and Vorobyov, 2005), and it remains unclear whether the arguments supporting the feed-forward hypothesis, which were based on analysis of responses to drifting gratings, would apply to the thin bar stimuli used by MacEvoy et al. (2009). In addition, normalization is observed in a variety of visual cortical computations in both V1 and MT (Heuer and Britten, 2002), and experiments and circuit models suggest that recurrent cortical

connections, particularly those that operate in an inhibition-stabilized regime (Ozeki et al., 2009; Shushruth et al., 2012; Rubin et al., 2015; Litwin-Kumar et al., 2016; Sato et al., 2016; Palmigiano et al., 2020), have the necessary ingredients to implement normalization that does not involve direct cross-orientation inhibition.

We designed experiments to directly probe the possible role of cortical circuits in cross-orientation normalization. Using a custom ProjectorScope apparatus (Huang et al., 2014; Roy et al., 2016), we located orientation maps in ferret visual cortex with intrinsic signal imaging, and then provided patterned optogenetic stimulation directly to different orientation columns. We examined, with electrode recordings, how cortical circuits integrate visual and optogenetic stimuli of different contrasts and orientations.

We observed substantial differences in the interaction of columns depending upon whether stimulation was delivered visually or optogenetically. First, optogenetic activation of an orientation column caused spiking activity that spread beyond the orientation columns that were directly stimulated (but not when glutamatergic synapses were blocked). Second, paired responses to visual stimulation at the preferred orientation and optogenetic stimulation of the orthogonal columns were smaller than the linear sum of the two stimuli alone, but the paired suppression was substantially less than was observed with purely visual paired stimuli. Further, paired optogenetic stimulation of iso-orientation and orthogonal columns showed far less suppression than visual-opto stimulus pairs. Finally, all 3 combinations of stimuli exhibited different suppression dynamics for marginal increases in the orthogonal stimulus, suggesting that different circuit behaviors underlie these different situations.

In a second set of experiments, we looked for hallmarks of inhibition-stabilized activity, where providing additional drive to inhibitory neurons causes a "paradoxical" decrease in inhibitory responses instead of the expected increase due to the increased drive (Tsodyks et al., 1997; Ozeki et al., 2009; Sanzeni et al., 2020). In models, the paradoxical decrease is due to a temporary increase in inhibition, which removes excitatory drive from the circuit, which in turn results in weaker activation of inhibitory neurons. Using an inhibitory cell specific promoter (Dimidschstein et al., 2016), we provided optogenetic activation to cortical inhibitory neurons during visual stimulation. We observed a range of inhibitory neuron responses, including some that were "paradoxical" and others that were not.

Results

Direct stimulation to test normalization mechanisms in cortex

Visual cortical neurons exhibit sublinear responses to the simultaneous presentation of two grating stimuli (Adelson and Movshon, 1982; Morrone et al., 1982; Morrone et al., 1987; DeAngelis et al., 1992; Heeger, 1992; Carandini et al., 1997; Simoncelli and Heeger, 1998; Reynolds and Heeger, 2009; Popovic et al., 2018), Because some of this suppression is likely present in the inputs to the cortex that arise from LGN (Freeman et al., 2002; Li et al., 2006; Priebe and Ferster, 2006), we designed an experiment to directly provide input to different regions of the cortical circuit itself, in order to separate cortical contributions to normalization from those of its inputs.

To do this, we updated a custom-made optical system (Roy et al., 2016), now called ProjectorScope 2 (Fig. 1A), that allowed us to use intrinsic signal imaging (Blasdel and Salama, 1986; Grinvald et al., 1986) to identify the locations of orientation columns and also allowed us to provide patterned optogenetic stimulation to the cortical surface. We injected viruses to express a variant of ChR2 (Boyden et al., 2005; Berndt et al., 2011) nonspecifically in all neurons (Roy et al., 2016) and prepared the ferrets for intrinsic signal imaging. After the orientation column map was acquired, optogenetic stimulation masks that targeted certain orientation columns were calculated based on the empirical map, and masked images were subsequently projected onto the V1 surface to stimulate the corresponding columns (Fig. 1B and 1C).

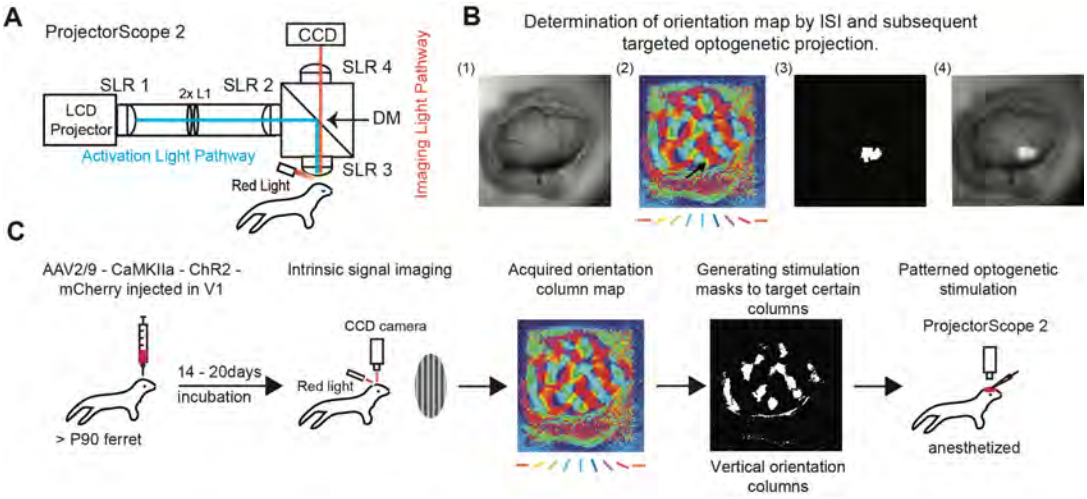

Figure 1. Optogenetic simulation of functionally-identified cortical columns with ProjectorScope 2. A: ProjectorScope 2 construction. Patterned light for optogenetic stimulation is generated by an LCD projector and transmitted to the brain surface by three SLR lenses of the same type. Two juxtaposed lenses (2x L1) are used to minify the projection image to the appropriate size, 3mm by 3mm, in order to target several orientation columns in ferret V1. A dichroic mirror (DM) reflects light between 390-460 nm to activate ChR2, while allowing green and red light to pass to the CCD camera for intrinsic signal imaging (ISI). ISI is performed by providing brightfield red light over the brain surface and taking images of the reflected light using the CCD, with an SLR lens to bring the light into focus. **B:** Determination of orientation map by ISI and subsequent targeted optogenetic projection. (1) Brain surface lit by room light. (2) The orientation column map acquired by ISI. The color key indicates the angle that a local region prefers. The arrow points to a region that will be used for targeted projection. (3) A projection mask based on the region pointed by the arrow in (2). (4) A raw image of the projection of the mask onto the brain surface. **C:** Viruses are injected to express ChR2 in V1 of adult ferrets, over 90 days old. After about three weeks, ISI is performed on the transfected ferrets to acquire an orientation column map. Then, the masks that target columns with certain orientation angles are generated based on the map.

Single-column optogenetic stimulation causes wide spread of activity due to horizontal connections

A key requirement of our experiment was to demonstrate that we could provide distinct input to different groups of nearby cortical neurons. While it was clear from visual inspection of the camera image that the light stimulus was illuminating distinct portions of the cortical circuit, several outcomes were possible at the neural level. First, providing direct input to a small column of neurons might only activate the neurons that were stimulated. Second, our direct optogenetic input might be restricted to distinct groups of neurons, but that activity could spread across columns through cortical synaptic connections; in this case, we would need to perform additional experiments with synaptic blockers to show that optogenetic inputs were being provided to distinct groups of neurons. Third, because axonal projections extend for millimeters and dendritic trees extend for a few hundred microns across the cortical surface, activation of these axons and dendrites might be sufficient to drive spiking in cell bodies over a wide area, which would mean that we would be unable to provide inputs to distinct groups of nearby neurons even with precise optical stimulation of the cortical surface.

Using electrodes, we characterized the optogenetic receptive zone (ORZ) of single neurons by stimulating the brain surface using circular dots ($\approx 750\mu m$ in diameter) in a randomized fashion. A 2-D Gaussian fit was performed on the recorded optogenetic responses over the cortical surface to delineate the local region that could be effectively activated by light (Fig. 2A). The ORZ could therefore be described as an elliptical shape comprising the interior 63%-tile of the fit (Roy et al., 2016).

We found that ORZs were larger in these adult ferrets (about the size of a ferret hypercolumn) than in our previous work in young ferrets (Roy et al., 2016), so we created stimuli to test the specificity of

activation of different orientation columns that were restricted to the ORZ (Fig. 2B). In this manner, we examined the "tuning" of each neuron to optogenetic activation of various orientation columns within the ORZ. We found that responses were quite non-specific, indicating that cortical activity spread substantially across orientation columns (Fig. 2C, left). There are two possible sources for this spread: either our optical stimulus itself caused widespread activation, or direct optogenetic activation was restricted to specific regions of the cortical surface and the spread of activity was due to activity within the cortical network.

To differentiate the two scenarios, we applied synaptic blockers (NBQX and DL-AP5 to block AMPA and NMDA receptors, respectively) and measured the specificity index (1- circular variance) before and after the application of synaptic blockers. We found that neurons exhibited more specific responses to the preferred-column activation in the presence of synaptic blockers (Fig. 2D, t-test, P = 0.0387). This suggests that some of the non-specific column-based optogenetic stimulation is due to the spread of evoked neural activity via connections intrinsic to the visual cortex, consistent with previous studies in tree shrew (Huang et al., 2014). Nevertheless, the fact that responses evoked with optogenetic stimulation in the presence of synaptic blockers were more local showed that we were able to provide input to distinct regions.

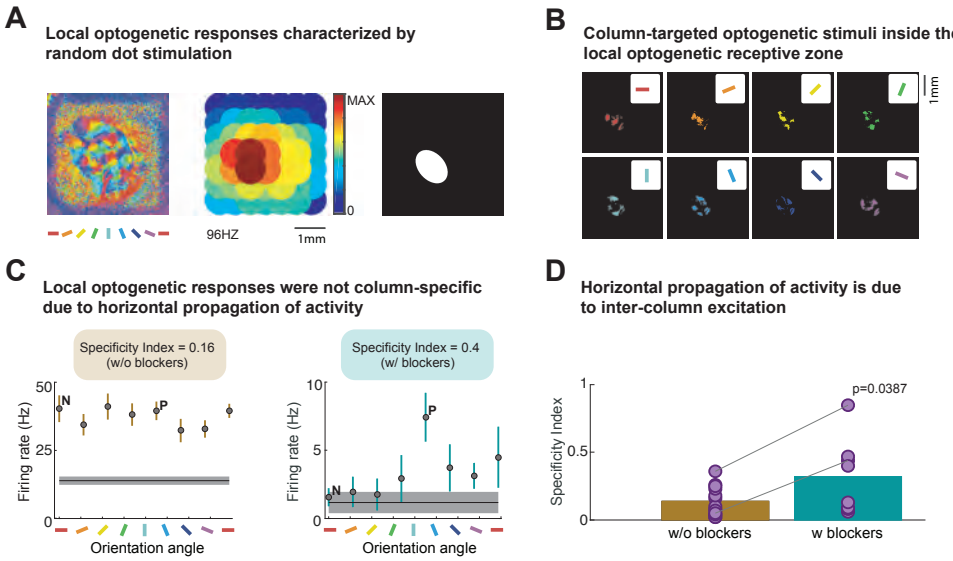

Figure 2. Although optogenetic activation of cortex produced local activity, this activity did not respect boundaries of orientation columns, due to horizontal propagation of activity. A: The orientation column map (left); the optogenetic responses of a single unit to spot stimuli (750 μm in diameter) with the heat map indicating the response intensities (middle); the elliptical optogenetic receptive zone (ORZ) characterized by two-dimensional Gaussian fit of the responses to spot stimulation (right). **B:** The masks used to test the orientation column specificity of the optogenetic stimulation were generated inside the optogenetic receptive zone and targeted orientation columns of varying angles with steps in 22.5 degrees. **C:** A neuron's optogenetic responses of the orientation specificity test before synaptic blockers and after synaptic blockers. The orientation angles shown on the x-axis are the angles of the corresponding column masks. **D:** The average specificity index of all the neurons (n=12 without blockers; n=8 with blockers) after synaptic blockers are applied is higher than that when no blockers are used (P<0.05). Blue lines connect data points acquired from the same neurons. These results imply that ChR2 stimulation of the cortex in animals of this age activates several adjacent orientation columns, in part due to synaptic propagation of signals across the cortex.

Visual, mixed visual and optogenetic stimulation, and paired optogenetic stimulation have different normalization properties

Having established that we could provide distinct independent inputs to different groups of cortical neurons, we examined the cortical contributions to normalization by comparing how the re-

sponse to the simultaneous presentation of a pair of stimuli was related to a simple linear sum of the responses to the stimuli independently. In all, we compared cortical integration under three conditions: visual, combined visual and optogenetic, and all optogenetic (Fig. 3).

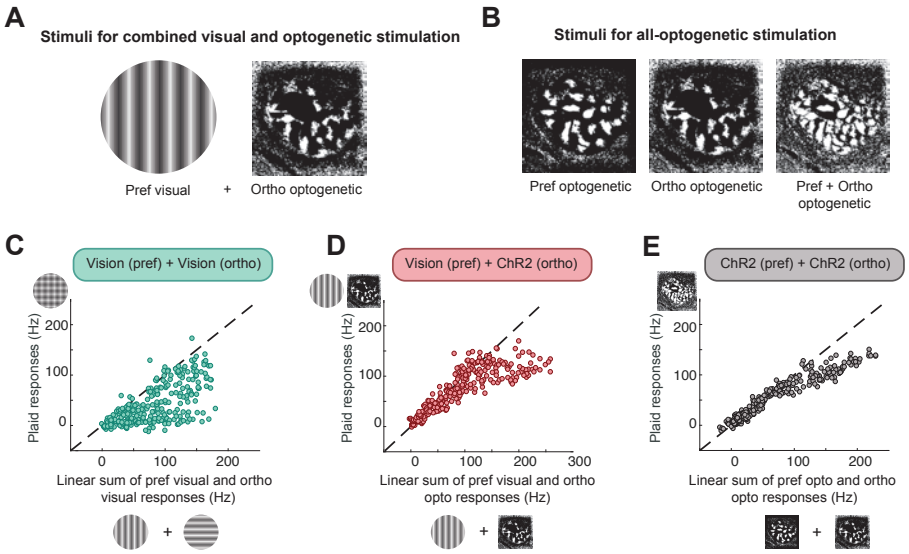

Figure 3. Neurons exhibit sublinear responses to combined visual and optogenetic stimulation. A: The stimuli used for hybrid stimulation. The visual stimulus provides the preferred orientation of the recorded neuron and the projection mask provides optogenetic modulation. **B:** Optogenetic stimuli for activation of neuron recorded with an electrode. Left) A strong optogenetic stimulus that includes the electrode region and all columns that prefer the same orientation (within 30°) as the recording site. Middle) A modulating stimulus that excludes the 1-sigma optogenetic receptive zone but includes all columns that prefer the orthogonal orientation (within 30°) as the recording site. Right) Combined stimuli. **C:** Single-unit responses to paired visual stimulation of preferred and orthogonal orientations, compared to the linear sum of preferred and orthogonal responses when those stimuli were presented alone. For each cell (N=23 cells, from 5 animals), responses to 16 combinations of preferred and orthogonal orientations are shown (4 contrast levels each). Responses are clearly sublinear for stimuli that evoked low or high firing rates. **D:** Single unit responses to paired visual and optogenetic stimulation. For each cell, responses to 16 combinations of visual preferred orientation (4 contrast levels) and optogenetic stimulation of the orthogonal orientation columns (4 drive levels) are shown. For stimuli that evoked low firing rates, paired stimulation exhibited mostly linear summation, but this summation became more sublinear for stimuli that evoked higher firing rates. **E:** Single unit responses to optogenetic stimulation of a cell's preferred columns and orthogonal columns. For each cell, responses to 16 combinations of optogenetic drive (4 drive levels for preferred stimulation and orthogonal stimulation) are shown. For stimuli that evoked low firing rates, paired stimulation produced a response that was nearly the same as the linear sum of the two component stimuli when presented alone. For stimuli that evoked larger responses, summation became non-linear.

In the first condition (all visual), we examined the classic phenomenon of cross-orientation suppression by comparing the sum of the responses of neurons to visual stimulation at the preferred orientation or at the orthogonal orientation to the response to a visual "plaid" of the two orientations presented together, at a variety of stimulus contrasts. We compared these results to stimulation with a visual stimulus at the preferred orientation combined with optogenetic activation of the orthogonal orientation columns (Fig. 3A). Once again, we varied the relative drive of these stimuli, by varying contrast in the case of the visual stimulus and by varying optogenetic light intensity in the case of the optogenetic stimulus. Finally, we examined the responses to optogenetic stimulation of columns that matched the preferred orientation of the recorded cell, optogenetic stimulation of columns that were orthogonal to the preferred orientation of the recorded cell, and responses to both stimuli paired, at a variety of optogenetic stimulus intensities (Fig. 3B).
There were obvious differences in the interactions among the different stimulation conditions. Responses of all recorded cells (N=23) to all contrast combinations are shown in Fig. 3CDE. Cross-

orientation visual stimulation showed substantial non-linear summation at all contrast levels and response intensities (Fig. 3C), while visual-optogenetic or optogenetic-optogenetic stimuli combined linearly at low-to-moderate response levels and then exhibited sublinear summation at high response levels (Fig. 3DE).

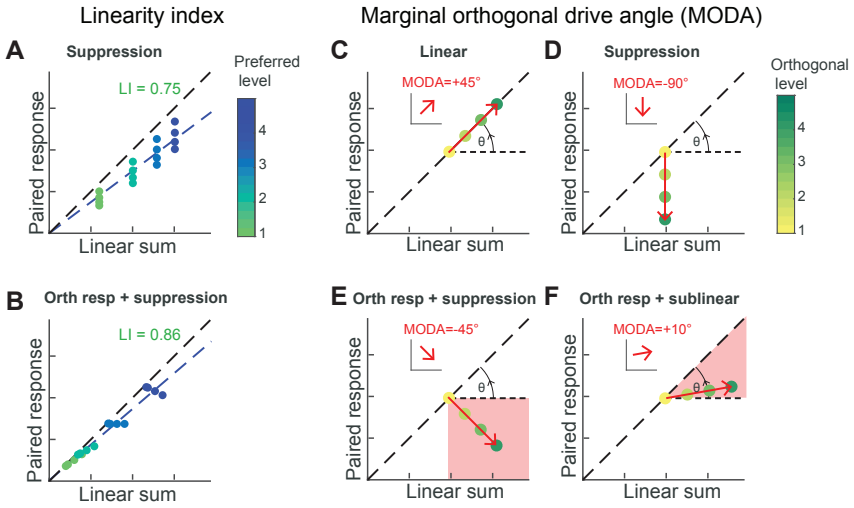

Figure 4. Single unit response schematics. **A:** Responses of a schematized neuron to paired stimulation of a preferred and orthogonal stimulus, as compared to the linear sum of responses to the individual stimuli alone. The schematized neuron was stimulated with the preferred stimulus at 4 levels of drive α_1 – α_4, and the orthogonal stimulus also covaried with 4 levels of driveβ_1 – β_4. Color indicates the preferred stimulus contrast. We calculated a Linearity Index (LI) as the slope of a linear fit that went through the origin and fit the other points with least squared error. **B:** A second schematized neuron. **C-F**: A neuron being driven with a high-drive (α_4) preferred stimulus paired with an orthogonal stimulus at increasing drive (β_1 – β_4). **C:** In this neuron, the response to paired stimulation is equal to the linear sum of the stimuli presented alone; that is, for marginal increases in orthogonal drive (increases in β), the response moves at an angle of +45° in this space. We call this the Marginal Orthogonal Drive Angle (MODA). **D:** An example of pure suppression. Marginal increases in orthogonal stimulus drive causes a reduction in the paired response, but the orthogonal stimulus does not provide any drive by itself (linear sum of the two stimuli alone is unchanged). MODA is -90°. **E:** A cell where the orthogonal stimulus produces a response alone – the responses move rightward along the X axis with increasing orthogonal drive – but the net impact on paired stimulation is to provide suppression – the response moves downward along the Y axis with increasing orthogonal drive. MODA is between -90° and 0°. **F:** A cell where the orthogonal response produces a response alone and the net impact on paired stimulation is sublinear addition – the response moves rightward and upward with increasing orthogonal drive. MODA is between 0° and +45°.

To probe these differences further, we developed two quantitative measures. The first measure, that we termed the Linearity Index (LI), is a measure of the overall linearity of the response and is the slope of the line that i) must pass through the origin at 0,0, and ii) passes through all responses to all combinations of paired stimuli with least squared error (Fig. 4AB). For the second measure, we calculated the directional angle of movement of the joint response vs. the linear sum of responses when the preferred contrast was high as the orthogonal contrast was increased (see Materials and Methods). We called this second measure the Marginal Orthogonal Drive Angle (MODA). A MODA value of +45° indicates linear summation (Fig. 4C), while a MODA value of -90° indicates that the second stimulus does not exhibit a response on its own but provides suppression of the response to the first stimulus (Fig. 4D). MODA values that are between -90° and 0° indicate that the second stimulus does exhibit some response on its own, but that its influence on the paired stimulation is overall suppressing (Fig. 4E). Finally, MODA values between 0° and +45° indicate that the second stimulus exhibits some response on its own, and contributes positively but sublinearly to the response to the paired stimuli (Fig. 4F).

Analysis of single cell responses indicated that normalization was substantially different across

these different stimulus conditions. In the all-visual condition, responses were highly sublinear across all response intensities, and orthogonal stimuli tended to be primarily suppressive (MODA near -90°), as shown in the example cells in Fig. 5A. In the mixed vision-optogenetics condition, responses were relatively linear for low stimulus response values. Many cells, such as those examples in Fig. 5B, exhibited MODA values between -90° and 0°, indicating that the orthogonal optogenetic stimulus provided some response on its own, but that this orthogonal stimulus most commonly provided suppression to the paired stimulation. In all-optogenetic stimulation (Fig. 5C), MODA values were commonly just slightly positive, indicating that orthogonal stimulation provided a response when presented alone, and that the paired response was increased by orthogonal stimulation, albeit in a sublinear manner.

Population data across all cells is shown in Fig. 5DEF. In the all-visual condition, the Linearity Index (LI) was statistically constant (Fig. 5Di), being the same for cells that exhibited low firing rates or high firing rates when the preferred stimulus was shown at high contrast (P=0.6149). The MODA values in the all-visual condition were clustered around -90° (Fig. 5Dii), indicating that the orthogonal visual stimulus did not drive cells by itself, but suppressed responses to preferred visual stimuli. This was true particularly for cells with long Marginal Orthogonal Drive vector lengths that reflect the presence of a strong trend. In the mixed visual and optogenetics measurements, the linearity index was nearly 1 for cells that exhibited lower firing rates to high contrast visual stimulation, but was less than 1 for cells that exhibited higher firing rates to high contrast visual stimulation (Fig. 5Ei). MODA values for this condition were variable, with most cells ranging between -90° and 0° (Fig. 5Eii), indicating that the orthogonal optogenetic stimulus drove cells by itself, but suppressed responses to preferred visual stimuli. Finally, for the all-optogenetic condition, linearity indexes were again dependent upon the maximum firing rate of the cell to the preferred stimulus, with cells that exhibited high firing rates exhibiting more sublinear responses (Fig. 5Fi. MODA values were clustered around a slightly positive angle (Fig. 5Fii), indicating that the orthogonal optogenetic stimulus drove cells by itself, and added sublinearly to the response to preferred optogenetic stimuli. The different MODA values across the three stimulus pairing types indicated that these results cannot be explained by a simple single-cell saturation mechanism, but rather suggest that cortex is integrating these signals differently.

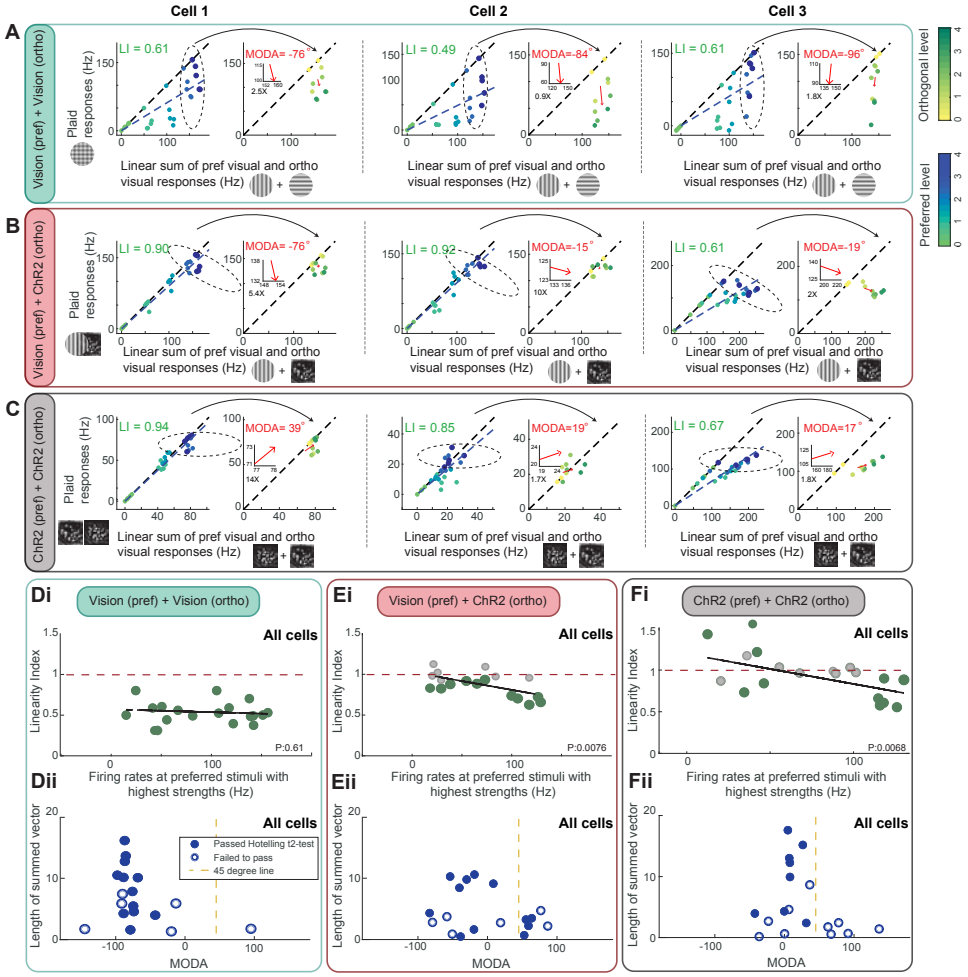

Figure 5. Responses of individual neurons and populations. A: Responses to paired visual stimulation of preferred and orthogonal gratings compared to the linear sum of those stimuli delivered alone. **A, left graph**: Cells were shown preferred gratings at 4 different contrast levels (levels, see color key) and orthogonal gratings at 4 different contrast levels (not differentiated). Linearity index (LI) fit line shown with LI value.**A, right graph**: Changes in responses with marginal increases in orthogonal drive. Responses to increasing orthogonal drive are shown paired with the two highest preferred contrasts. Marginal orthogonal drive vector and marginal orthogonal drive angle (MODA) indicated. A zoomed-in view of the MODA vector is provided in the inset, with magnification (NX) indicated. Note how for cell 2 and 3, the MODA is close to 90°, indicating almost pure suppression. **B:** Same, but for combinations of visual and optogenetic stimulation. Cells were driven with visual gratings at the preferred orientation with 4 levels of contrast, and orthogonal orientation columns were driven optogenetically at 4 levels of drive. Cells in B are the same cells in A. MODA values were variable among this population. **C:** Same, but for all optogenetic stimulation. Cells were driven with optogenetic stimulation of the preferred columns at 4 levels of drive, and were driven with optogenetic stimulation of the orthogonal columns at 4 levels of drive. MODA values tended to be above 0°, indicating that orthogonal stimuli provided drive and added sublinearly with the preferred stimulus. **Di,Ei,Fi**: Linearity index values for all cells, plotted against the firing rate that was produced for preferred stimuli at the highest contrast or drive. Di: For purely visual stimulation, Linearity Index values were approximately 0.5 and did not exhibit any significant correlation with maximum firing rate (Pearson's correlation, p=0.615). Filled dot indicates values that differed significantly from 1 (t-test, $p<0.05$). Open dot in subsequent panels indicates values that did not differ significantly from 1 (t-test, $p<0.05$) **Ei**: For mixed visual and optogenetic stimulation, Linearity Index values were approximately 1 when cells exhibited low firing rates, and decreased when cells exhibited higher firing rates. There was a significant correlation between the Linearity Index and maximum firing rate for visual stimulation at the preferred orientation (Pearson's correlation, $p<0.0076$). **Fi**: Linearity index values when stimulation to preferred and orthogonal columns was provided by optogenetic stimulation. There was a significant correlation between the Linearity Index and maximum firing rate ($p<0.0068$). **Dii,Eii,Fii**: Marginal orthogonal drive vector lengths and angles.

Fig. 5 Caption continuation Cells that exhibited a vector that differed significantly from 0,0 (Hotelling-T2 test $p<0.05$) are indicated by filled dots; vectors that did not differ significantly from 0,0 are plotted as open dots. **Dii**: Length and MODA values for visual stimulation. There were a cluster of points with significant vector lengths with MODA values near -90°, indicating that cross-orientation stimulation is primarily suppressing. **Fii**: Values for mixed visual stimulation (preferred orientation) and optogenetic stimulation (orthogonal columns). There was a range of MODA values but the median cell exhibited a MODA value that was between -90° and 0°. **Gii**: Values for optogenetic stimulation (preferred columns and orthogonal columns). MODA values for vectors that had significant length were slightly positive. These results indicate that all three stimulus paradigms exhibited different marginal influences of increasing orthogonal drive.

Circuit models that might underlie these responses

At first inspection, the differences in normalization for these different conditions are difficult to reconcile with what is known from previous work on cortical circuits. If we imagine a region H that is selective to horizontal orientations, and a nearby region V that is selective to vertical orientations, then during visual stimulation with horizontal orientations, region H exhibits strong responses, while region V does not respond. Further, synaptic conductance measurements of visually responsive neurons in region V indicate that principal neurons in V do not receive strong inhibitory or excitatory inputs when horizontal orientations are presented (Anderson et al., 2001), so the visually responsive neurons in H cannot strongly inhibit or excite the principal neurons of V. On the other hand, if we optogenetically activate region H, then we observe responses in V.

How can optogenetic activation of region H cause activity in region V when visual activation of H does not? If we set aside the possibility that the direct optogenetic stimulation is not actually local (see Fig. 2), then one of the simplest ways this can happen is if there are projections across the columns by neurons that are not driven by the visual stimulus used to drive area H. These neurons might not be visually responsive at all, or might have spatial or temporal frequency preferences that were not driven by the visual stimuli used here. A 2-photon imaging study of anesthetized ferrets of a similar age showed that visual responses are relatively sparse, and that many neurons did not exhibit responses to visual stimulation (Smith et al., 2015). These neurons are likely to be activated by optogenetic stimulation, and they may exhibit coupling into the circuit that differs from their nearby visually-active neighbors.

There is a wide – but not an unlimited – number of possible circuits that could meet these criteria. Here, we show two examples of circuit models that are inconsistent with our observations on the way to unpacking one example circuit configuration that is consistent with our observations.

We began with the ring model of Rubin et al. (2015) (Fig. 6A). Each position in the ring represents a preferred orientation, ranging around the ring from 0° (= 180°) to 179°, and is modeled by a pair of E and I cells that are reciprocally- and self-connected. Each pair forms a supralinear stabilized network. The synaptic strengths of the horizontal connections across elements of the ring fall off slowly with distance/orientation in a gaussian manner, and all connection strengths (E-to-E, E-to-I, I-to-E, I-to-I) fall off with the same distance dependence (σ = 32°, as one moves along the ring). The visual input is tuned to stimulus orientation and falls off in a Gaussian manner (σ = 30°) as one moves away from the cells that prefer a given orientation, and optogenetic input falls off similarly but is set slightly broader (σ = 45°). The visual and optogenetic input are provided to both E and I cells. Neurons with different maximum firing rates are simulated by varying the maximum input level provided to different simulations.

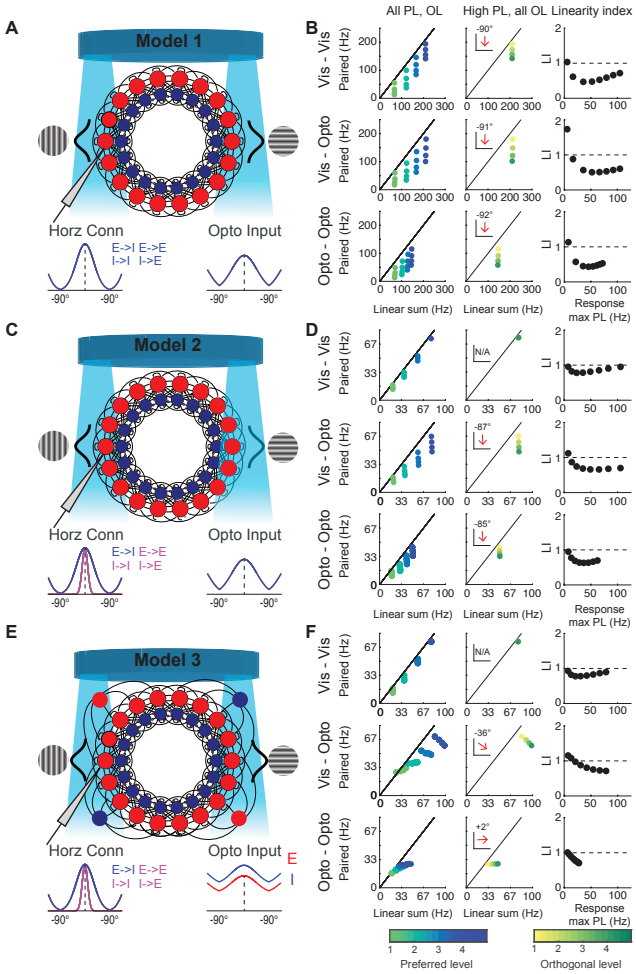

Figure 6. Models consistent with data. Common to all models: Cells are arranged in a ring, with an excitatory (E) and inhibitory (I) unit at each position. Position corresponds to preferred orientation. The units are coupled in a supralinear stabilized network. Visual and optogenetic inputs are centered at the stimulus orientation, are equal to E and I units at a given position, and decrease as a Gaussian function of the difference between the stimulus orientation and the units' preferred orientation. For visual input, the Gaussian has standard deviation 30°; for optogenetic input, the standard deviation is 45°. **A:** Model 1: The ring model of Rubin et al. (2015). Horizontal connectivity among all cortical cells decreases as a Gaussian of standard deviation 32°. **B:** Left) Responses of Model 1 to stimulation with 16 combinations of 4 preferred levels of drive (PL) and 4 orthogonal levels (OL) of drive. Cells were shown preferred gratings at 4 different contrast levels (levels, see color key) and orthogonal gratings at 4 different contrast levels (not differentiated) Top) preferred and orthogonal are visual; Middle) preferred is visual and orthogonal is optogenetic; Bottom) preferred and orthogonal are optogenetic Center) Responses for the strongest preferred stimulus and varying orthogonal drive (see color key). MODA value indicated in inset. Right) Linearity index for cells with different maximum firing rates. Model 1 exhibits stronger normalization than is observed in cortex, and marginal orthogonal drive increases cause only suppression, in contrast to data from cortex for visual-optogenetic and optogenetic-optogenetic conditions. **C:** Model 2: Modified ring model with less cortical normalization. Now, E to I connections fall off as a Gaussian of 25° width; other connections fall off with 10° width. **D:** Same as B, for Model 2. Visual normalization is no longer provided by the cortex. For optogenetic stimulation, this model exhibits weaker normalization, but orthogonal stimuli are still almost purely suppressing, in contrast to data from experiments. **E:** Model 3: Now optogenetic stimulation also activates non-visual E and I neurons (disembodied cells) that are coupled to the entire network, so that the effective optogenetic input is broad. **F:** Same as B, for Model 3. Now, mixed visual and optogenetic input is more linear at low responses, and MODA shows that the orthogonal stimulus provides some response by itself but suppresses responses to the preferred visual stimulus, as in experiment. Pure optogenetic stimulation is more linear at low response rates, and MODA shows that the orthogonal stimulus provides some response by itself and adds sublinearly to the response to the preferred visual stimulus, as in experiment.

Responses to combinations of visual and optogenetic inputs at different contrasts in the unmodified Rubin et al. (2015) (Model 1) are shown in Fig. 6B. Previous studies (Ahmadian et al., 2013; Rubin et al., 2015) have shown that cross-orientation normalization in this model occurs alongside the paradoxical response of an inhibition-stabilized circuit: cross-orientation inputs to inhibitory neurons causes the firing rates of both E and I neurons to drop, so that overall cross-orientation suppression results in a net reduction of both excitatory and inhibitory synaptic conductances. In this model, linearity indices are near 1 for cells that were only driven weakly by the preferred stimulus, and drop to about 0.5 for cells that are driven more strongly by the preferred stimulus. This differs from the actual data from our experiment, where the linearity index was nearly constant (around 0.5) for cells that were driven either strongly or weakly (Fig. 5D). Further, MODA values in the model for all conditions (all-visual, mixed visual and optogenetic, and all-optogenetic) were all around -90°, indicating that the orthogonal stimulus was producing strong suppression without causing a response on its own. These simulation results are inconsistent with our measurements in the mixed and all-optogenetic conditions (where the orthogonal stimulus caused a response and MODA > -90), indicating that the unmodified Rubin et al. model exhibits stronger cross-orientation normalization than we observe in our measurements.

The fact that normalization in the original Rubin et al. model was too strong to account for the mixed visual and optogenetics results led us to explore a different cortical circuit model (Model 2). We dropped the requirement that the cortical circuit itself should provide visual cross-orientation suppression; instead, we allowed our model circuit to exhibit little visual cross-orientation suppression, assuming that in the real circuit, much or all of this might occur in feed-forward inputs from the LGN (Freeman et al., 2002; Li et al., 2006; Priebe and Ferster, 2006; Priebe, 2016). We modified the model so that E-to-E, I-to-E, and I-to-I connections were all much more local (10° Gaussian fall-off instead of 32° fall-off), while leaving E-to-I connections at a 25° fall-off to allow some within-cortex normalization (Fig. 6C) but much weaker than would be required to account for cross-orientation suppression. Simulations showed that this model still lacked important features of our data: optogenetic cross-orientation stimulation did not, by itself, evoke strong responses in the model as it did in our data, but instead exhibited almost pure suppression (Fig. 6D). In this model, cross-column suppression when using an optogenetic stimulus is due to the broader tuning of the optogenetic input (σ = 45°).

Finally, we examined a circuit (Model 3) that had additional E and I neurons that were not visually active (Fig. 6E). Presumably these non-visual cells are active under specific conditions that might involve other modalities or modulatory states. We made very simple assumptions about these non-visual E and I neurons: they did not receive input from visually-responsive neurons, but they did provide broad, uniform projections to visually-responsive neurons around the ring. This model exhibited several features of our actual data (Fig. 6F). First, single optogenetic stimuli directed at preferred or orthogonal columns evoked responses across the whole ring. Second, mixing a preferred visual stimulus with optogenetic stimulation of the orthogonal orientation columns evoked suppressive responses (MODA angles less than 0°). Third, normalization was relatively linear for neurons that were driven to low firing rates (response ratio approximately 1 or even higher), and the degree of suppression increased for neurons that were driven to high firing rates (response ratio less than 1). Normalization was only prominent when cells were driven to higher firing rates, similar to the actual data. Fourth, paired optogenetic stimulation evoked sublinear responses but exhibited positive MODA angles (greater than 0°), indicating that the paired response was greater than the response to the preferred stimulus alone.

Selective optogenetic stimulation of inhibitory neurons reveals broad classes of functional types.

While Model 3 is consistent with our data, the space of possible cortical circuits that might exist in the brain and be consistent with our data is still very large. We sought to look for direct evidence of the inhibition-stabilized dynamics that the model posits, as has been found in the mouse (Sato

et al., 2016; Adesnik, 2017; Sanzeni et al., 2020) and for which evidence has been reported for surround suppression in cat (Ozeki et al., 2009) and ferret (Rubin et al., 2015). A key prediction of ISN-type dynamics is the presence of so-called "paradoxical responses" (Ozeki et al., 2009). If network activity is driven strongly by recurrent connections among excitatory and inhibitory cells, then local excitatory cells are responsible for a significant portion of the synaptic drive to inhibitory cells. If one were to selectively deliver an increase in drive to inhibitory neurons, then excitatory neurons would slow down, but this reduction in excitatory drive would in turn reduce the activity of cortical interneurons. Hence, in the model, the inhibitory cells "paradoxically" respond to small increases in activation with overall reductions in activity (as compared to the increase in activity that might be naively expected).

This prediction is illustrated by simulations in Fig. 7. Under a parameter regime where excitatory recurrent connections are set so strongly that the network activity would blow up without inhibition, and inhibitory synaptic strengths are set to be high enough to stabilize this activity (ISN regime), an external increase in drive to inhibitory neurons results in the described paradoxical decrease in activity in interneurons, until the external optogenetic drive to the inhibitory interneurons becomes so strong as to dominate the interneuron responses (Fig. 7ABC, same parameters as a single column of the rings of Rubin et al. 2015 and Model 3). On the other hand, if recurrent connections among excitatory and inhibitory neurons are weak (non-ISN), then external drive to inhibitory interneurons merely serves to monotonically increase the activity of these interneurons (Fig 7DEF).

To test these predictions, we prepared ferrets with a virus (AAV9-mDlx-ChR2-mCherry-Fishell-3) that restricts the expression of channelrhodopsin-2 to inhibitory neurons (Dimidschstein et al., 2016). We delivered wide-field white light to stimulate the brain surface, and the light intensity was modulated to achieve different levels of external drive to inhibitory neurons. Optogenetic stimulation was presented with and without visual stimulation at the preferred orientation with different contrasts, in order to understand how the activated cortex would be modulated by the external optogenetic increases in inhibitory drive. In these experiments, a 32-channel probe (Plexon S-probe) was used to achieve better yield of recording both excitatory and inhibitory cells.

We observed a variety of response profiles to combined visual stimulation and optogenetic stimulation of interneurons. Some cells exhibited no response to optogenetic interneuron stimulation alone, but exhibited strong suppression of visual responses when optogenetic drive was strong. We labeled these neurons as putative excitatory neurons (Fig. 8A, bottom row).

We also observed response profiles that we imagined arose from inhibitory neurons. These cells, labeled as putative inhibitory neurons, exhibited strong responses to strong optogenetic stimulation when it was presented either with or without visual stimulation (Fig. 8A, top and middle rows). The putative inhibitory neurons always responded directly to light and, on average but not always, exhibited shorter spike duration than the putative excitatory cells (Supplementary Figure 8-1).

The putative inhibitory interneurons were not uniform in response profile, but instead exhibited a range of responses. At one extreme, responses from some putative inhibitory interneurons resembled the responses from interneurons in an ISN-like circuit (Fig. 8A, top row). During high contrast visual stimulation, the activity of these interneurons was suppressed for weak optogenetic activation, consistent with the idea that increased drive to interneurons was reducing excitatory activity, which in turn decreased recurrent inhibitory activity. Without simultaneous visual stimulation, these were less clear, given the low spontaneous firing rates of most neurons. At another extreme, we also observed several neurons that exhibited monotonic increases in responses to optogenetic drive (Fig. 8A, middle row). These results suggest that there are multiple ways in which interneurons can be interconnected with cortical circuits. The full range of tuning profiles that we observed is projected onto its first two principle components and plotted in Fig. 8B. Within the putative inhibitory population, the data are more consistent with a continuum rather than discrete clusters.

The diversity of responses from putative interneurons raises the question as to the nature of the

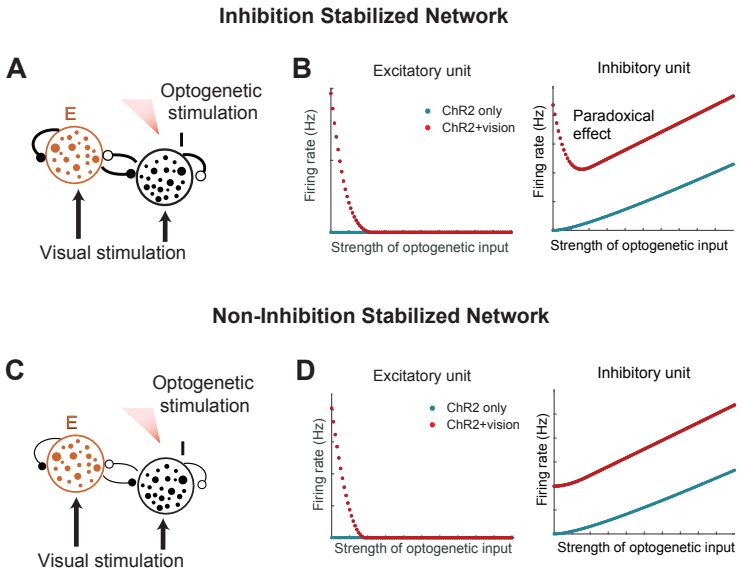

Figure 7. Differential responses to optogenetic interneuron stimulation in ISN and non-ISN models. A: In the simulation of ISN ring model (illustrated here as one pair of E and I), the E and the I units have strong recurrent connections. Visual stimulation provides inputs to both the E and the I units, and optogenetic stimulation provides inputs to the I units only. **B (left):** Excitatory unit responses in the ISN. When the inhibitory units are activated by ChR2 stimulation, the excitatory units have no responses. When visual stimulation is provided together with ChR2 stimulation, the excitatory units respond strongly to visual stimulation when the inhibition is weak and reduce firing rates as the inhibition becomes stronger. **B (right):** Inhibitory unit responses in the ISN. When the inhibitory units are activated by ChR2 stimulation but are not otherwise active in the circuit, they monotonically increase firing rates as the stimulation becomes stronger. When ChR2 stimulation is provided in the presence of visual stimulation, the firing rates decrease before increasing, creating a "dip" shape in the response curve that is characteristic of the ISN. **C:** In the simulation of the non-ISN model, the ring structure is maintained as in the ISN but the recurrent connections are weak. **D (left):** Excitatory unit responses in the non-ISN network. Activation of the interneurons suppresses the excitatory unit activity. **D (right):** Inhibitory unit responses in the non-ISN network. In the non-ISN network, the inhibitory units show direct responses to light in a monotonically increasing manner. When ChR2 stimulation is combined with visual stimulation, the inhibitory units also respond in a monotonically increasing manner and the "dip" is absent.

overall impact of cortical interneurons on the circuit. Of course, interneuron connectivity could be very specific, but as a point of interest we calculated the grand average of the normalized responses of all the inhibitory cells to combined optogenetic stimulation and visual stimulation (Fig. 8C). This grand average would reflect the inhibitory influence on the cortical network if interneuron types were pooled unselectively. The grand average tuning curve exhibits an empirical dip below zero for weak external input, although no point on the curve is significantly below 0 with a p-value of less than 0.05.

Diversity in interneuron responses to optogenetic stimulation could arise from diversity in the response of different inhibitory cell types, due to heterogeneity in neural connections, or due to the heterogeneity in the opsin expression across inhibitory cells. We created a large-scale EI network model with heterogeneous, randomly distributed connectivity (Fig. S4). We modeled the photocurrent to each cell as a Hill equation as reported experimentally (Asrican et. al. 2018), and the activation of each interneuron to vary with depth, as expected from scattering of light across the cortical tissue (Yona et. al. 2018). In this model, we observed a heterogeneous range of response profiles in optogenetically-activated interneurons, as in the data. The model not only captures the initial response of I cells to laser power, but also the negative correlation between the effect of the laser at low intensity and the effect of the laser at high intensity to each cell: If the cell is initially excited by the laser, then it tends to quickly saturate for large laser power, whereas if it responds

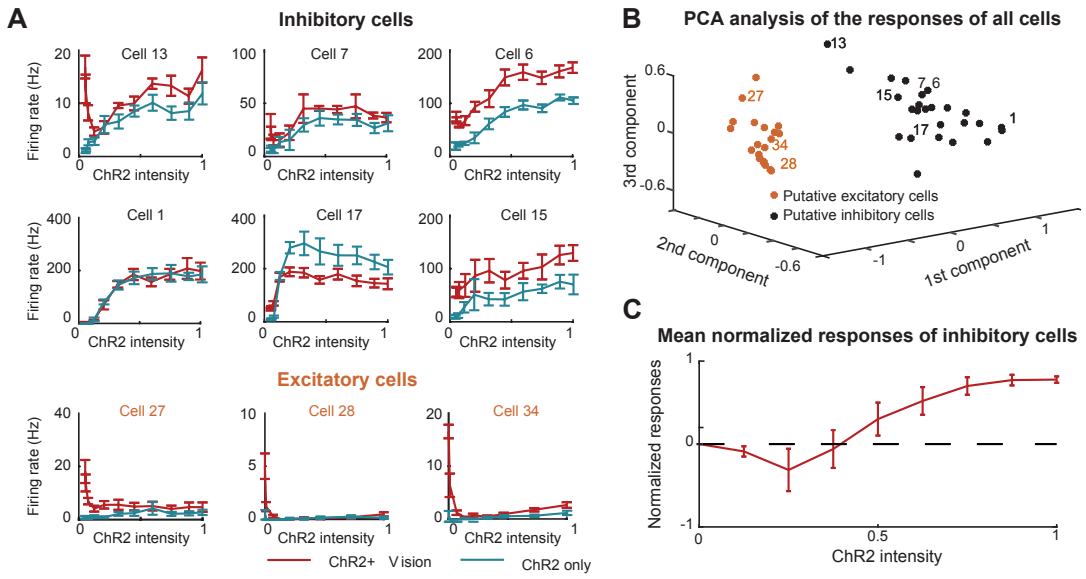

Figure 8. The influence of direct interneuron stimulation on visual responses in putative excitatory and inhibitory interneurons. A: Representative unit responses from the optogenetic inhibition experiments. Raw mean firing rates (without any background rate subtraction) are shown for increasing optogenetic stimulation alone (blue) or in the presence of a high contrast visual stimulus (red). Top) Putative inhibitory neurons that responded like neurons in the ISN simulation. Middle) Putative inhibitory neurons that did not respond like that the ISN simulation. Instead, the firing rates either saturated or increased at low light intensities and then decreased at high light intensities. Bottom) Putative excitatory neurons. **B:** Projection of response profiles to visual stimulation and increasing optogenetic interneuron activation onto the first 3 principle components. Putative excitatory and inhibitory neurons are well separated, but there is diversity of responses within the putative inhibitory population. Numbers indicate the example neurons displayed in **A-C** The grand average of the normalized ChR2+Vision responses of all putative inhibitory cells. For every inhibitory cell, the responses were normalized in such way that the average response at 0 light intensity is normalized to 0 and the average maximum response is 1.

paradoxically to the laser at low power (i.e. if it has a negative response to weak excitatory input) then its response does not saturate at large laser power. These results suggest that diversity in such properties as synaptic connectivity, optogenetic activation strengths, and cellular thresholds could underlie the variable response profiles we observed in Figure 8.

Discussion

In this study, we performed combined visual and patterned optogenetic stimulation to test how cortical circuits responded to multiple inputs. We found that cortical stimulation that was optically restricted to specific orientation columns caused activity that spread non-selectively to neighboring columns. We used this protocol to examine the cortical contributions to contextual modulation by stimulating different cortical columns visually and optogenetically. We found evidence for cross-column cortical normalization, but much less than would be needed for a purely cortical mechanism to account for cross-orientation suppression. We found a wide range of interneuron couplings to the circuit, including those that responded to weak optogenetic activation by reducing their activity, consistent with inhibition stabilized networks.

Nonspecific spread of activity with respect to orientation columns

We tested the spatial spread of optogenetic responses and found that the column-based patterned optogenetic stimulation did not respect the boundaries of orientation columns, although local activation was typically restricted around the recorded neuron. While it is difficult to exclude the possibility that this unselective spreading is due in part to activation of passing axons and den-

drites of neurons in other columns, blocking the NMDA and AMPA receptors revealed that the influence of horizontal connections played a large role. Viruses that cause strong expression of ChR2 that is targeted to the soma could help manage concerns about passing dendrites, but the one soma-targeting virus we were able to try did not cause sufficient expression to produce strong responses in vivo with our stimulation system (Baker et al., 2016). Our results are consistent with a study that performed sparse stimulation of nearby orientation columns in tree shrew (Huang et al., 2014). One might have expected to find species differences between tree shrew and ferret because the tree shrew primarily exhibits length-summation in layer 2/3 (Chisum et al., 2003) while ferret exhibits both length-summation and surround suppression (Rubin et al., 2015; Popovic et al., 2018), but both species showed non-specific spread of activity in layer 2/3.

An important corollary of nonspecific spread is that column-level stimulation of cortical neurons is unlikely to provide an optimal stand-in for visual activation, e.g. in a visual prosthesis. In addition, a given visual stimulus causes only a sparse activation of visual cortical neurons (Rochefort et al., 2009; Haider et al., 2010; Smith et al., 2015), and there appear to be cells that are not activated by visual stimulation or are only activated in conjunction with some non-visual stimulus (Saleem et al., 2018), whereas an optogenetic stimulus will activate all cells in a column. It is possible that expression of optogenetic channels restricted to LGN axons may allow more specific stimulation of visually-driven neurons in particular.

Linear vs. non-linear interactions of visual and optogenetic signals

Several studies have now examined integration of visual and optogenetic signals.

Huang and colleagues (Huang et al., 2014) used AAV viruses to cause very broad expression of channelrhodopsin in excitatory neurons in the tree shrew. In these experiments, optogenetic activation using small spots of light targeted to preferred or orthogonal columns added linearly over a wide range of firing rates. Further, visual stimulation with the preferred orientation combined with optogenetic stimulation of preferred columns also showed linear summation.

In macaque, Nassi et al. (2015) used lentivirus to cause more localized expression of C1V1 in excitatory neurons of the macaque. These investigators stimulated broadly with an optical fiber and observed a variety of facilitatory and suppressive interactions to joint visual stimulation and optogenetic stimulation that was not specific to particular columns of the orientation map. The vast majority of these neurons exhibited sublinear summation of visual and optogenetic signals.

Histed (2018) used transgenic approaches to cause expression of ChR2 in mouse visual cortical neurons, and found that visual and optogenetic inputs summed in a largely linear manner, though with sublinear summation at higher firing rates. Another study in the mouse, which used optogenetic antidromic activation of callosal inputs, found that callosal inputs facilitated responses at low visual contrasts but suppressed responses at higher visual contrasts (Sato et al., 2014).

We found evidence for nearly linear summation when neurons exhibited low firing rates, which became sublinear as neurons exhibited larger firing rates. These results cannot be explained by a simple process of single cell saturation of firing rate outputs, because marginal increases in orthogonal drive produced very different responses in the visual-optogenetic stimulation protocol as compared to the optogenetic-optogenetic stimulation protocol. This indicates a contribution of cortical circuits to this integration.

In layer 2/3, cross-column suppression is insufficient to account for cross-orientation suppression to visual stimuli

Cortical neurons exhibit weaker responses to a preferred oriented stimulus when the stimulus is combined with an orthogonally-oriented stimulus (Bishop et al., 1973; Morrone et al., 1982; Bonds, 1989; DeAngelis et al., 1992; Cavanaugh et al., 2002; Smith et al., 2006; Busse et al., 2009; MacEvoy et al., 2009). Experiments in the last 20 years have shown that direct cross-column inhibition is unlikely to underlie this phenomenon, as synaptic conductance measurements of both excitatory and inhibitory inputs peak at the preferred orientation and are relatively weak at the orthogonal

orientation (Anderson et al., 2000), and both excitation and inhibition are reduced by the addition of an orthogonal grating stimulus to a preferred-orientation grating stimulus (Priebe and Ferster, 2006).

A more recent model suggested that nonlinear circuit properties induced by supralinear single-cell input/output functions could explain the change from cross-orientation facilitation for weak stimuli to cross-orientation suppression for stronger stimuli. Furthermore, because the network was inhibition-stablized for stronger stimuli, the model could explain cross-orientation suppression with a combined reduction of excitatory and inhibitory conductances (Ozeki et al., 2009; Rubin et al., 2015). Cross-column excitatory inputs would cause inhibitory neurons to temporarily increase their firing rates, reducing the firing rates of their neighboring excitatory neurons. Because the neighboring excitatory neurons themselves provide strong input to their inhibitory neighbors, the overall firing rates of both excitatory and inhibitory neurons goes down, along with local excitatory and inhibitory synaptic conductances. Therefore, the model was compatible with the conductance measurements that did not show strong cross-orientation inhibition (Anderson et al., 2000; Priebe and Ferster, 2006).

Alternatively, other past models suggested that there was no need for any cortical explanation of cross-orientation suppression. These models suggest that cross-orientation suppression can be largely accounted for by changes in LGN inputs to V1 cells along with V1 spike threshold (Lauritzen et al., 2001; Freeman et al., 2002; Li et al., 2006; Priebe and Ferster, 2006; Priebe, 2016).

Our optogenetic stimulation results were inconsistent with a cortical explanation for cross-orientation suppression. Under the hypothesis that optogenetic stimulation is in any way like a visual stimulation, stimulation of orthogonal columns should have produced a strong suppression in the orthogonal columns. Instead, when we stimulated a set of orientation columns, we observed a moderate spreading of cortical responses. Combined visual and optogenetic stimulation produced responses very similar to the linear sum of the individual stimuli for moderate response strengths, while paired stimulation of visual stimuli of moderate contrast produced strongly sublinear responses. In our model that best matched the data, there was some weak cross-column suppression, but the cross-column suppression was much smaller than is required to produce the cross-orientation suppression seen using visual stimuli.

Inhibition-stabilized dynamics and paradoxical responses

Another goal of our study was to examine whether we could find direct evidence of inhibition-stabilized dynamics in ferret visual cortex. In inhibition-stabilized dynamics, the cortical circuit acts as a strong amplifier of external input, such that most of the synaptic drive that impinges on each cortical cell arises from within the cortex itself (Suarez et al., 1995; Tsodyks et al., 1997; Ozeki et al., 2009; Rubin et al., 2015). Evidence for inhibition-stabilized dynamics has been observed in studies of surround suppression in cat visual cortex (Ozeki et al., 2009) and mouse visual cortex (Sato et al., 2016; Adesnik, 2017; Sanzeni et al., 2020), mouse somatosensory cortex (Sanzeni et al., 2020), and mouse motor cortex (Sanzeni et al., 2020). Indirect evidence for inhibition-stabilized dynamics has been observed in ferret visual cortex (Rubin et al., 2015). Sanzeni et al (2020) also looked for paradoxical responses by direct optogenetic stimulation of interneurons, and found that paradoxical responses in awake animals could be evoked by stimulating either all interneurons or just PV neurons when they were targeted in a transgenic manner. Interneuron receptive field properties differ between species that have columnar features beyond retinotopic maps and those that only have retinotopic maps; for example, interneurons in cat and ferret visual cortex can be highly tuned for orientation (Hirsch et al., 2003; Cardin et al., 2007; Wilson et al., 2017), while a majority of interneurons in mouse visual cortex are not (Sohya et al., 2007; Niell and Stryker, 2008; Liu et al., 2009; Kerlin et al., 2010). Here we showed that a subset of ferret interneurons also exhibited characteristic paradoxical behavior with direct stimulation.

We observed heterogeneous interneurons responses to increasing optogenetic stimulation. These responses resemble the heterogenous paradoxical/non-paradoxical responses that Sanzeni et al.

(2020) and Mahrach et al (2020) observed in experiments using viral-mediated infection of PV+ neurons. Sanzeni et al. (2020) observed nearly universal paradoxical responses when they used transgenic methods to express optogenetic channels in either PV+ neurons or all interneurons, via a VGAT promotor. In ferret, we used a viral promotor that caused expression of ChR2 in a wide variety of interneuron classes (Dimidschstein et al., 2016), but interneuron subclass-specific viruses are now becoming available for non-rodents (Mehta et al., 2019; Vormstein-Schneider et al., 2020). Future experiments will be needed to determine if some of the heterogeneity we observed could be due to differences in responses of different interneuron subtypes.

Materials and Methods

General design.

All experimental procedures were approved by the Brandeis University Animal Care and Use Committee and performed in compliance with National Institutes of Health guidelines. Eleven adult ferrets (Mustela putorius furo, Marshall Farms; >P90, female) were used in total: five ferrets were used for patterned optogenetic experiments, four ferrets were used for optogenetic specificity experiments, and four ferrets were used for inhibitory optogenetic experiments. Females were used exclusively because co-housing male and female adult ferrets in the same space is stressful for the animals if they are not allowed to mate. For patterned optogenetic and optogenetic specificity experiments, AAV9.CamKIIa.hChR2(E123T/T159C).mCherry.WPRE.hGH was used to express ChR2 in neurons.

Virus injection.

All virus injections were achieved by pre-treating ferrets with ketoprofen (1mg/kg, IM) and tramadol (2-5mg/kg, oral) on the morning of surgery. The ferrets were anesthetized with ketamine/xylazine cocktail (20-30mg/kg, 2-3mg/kg) through IM injections and the anesthesia was maintained by additional injections of ketamine/xylazine (10-50% amount of ketamine/xylazine used during initial anesthesia). Atropine (0.16mg/kg) was given to reduce secretions. Ringer's solution (2.75/ml/kg/hr) was given by subcutaneous injections to prevent dehydration. The body temperature was controlled and monitored by a thermostatic controller (TR-200, Fine Science Tools or PhysioSuite, Kent Scientific), and the EKG levels were continuously monitored.

Ferrets were held in a stereotaxic apparatus by two ear bars and a bite bar. The heads were shaved and sterilized by alternate applications of Betadine-soaked gauze and 70% isopropanol-soaked gauze three times. Bupivacaine (0.25-0.5ml of 0.25% with a maximum does of 2mg/kg, IM) was injected around the incisions on the head. Head muscle and skin were retracted and a craniotomy, about 1-2 mm wide, was performed. A small durotomy was made with a 31-gauge needle on a cotton tip applicator. The glass pipettes used to inject viruses were pulled on a vertical puller (PC100, Narishige) and beveled to achieve a tip about 30um in diameter. Virus was delivered by a microinjection device (Nanoject, Drummond Scientific) with 22 pulses of 23 nl/pulse with 10 seconds intervals. To achieve a broad expression area (2.5 mm2), two or three locations were injected, two depths (300um and 500um below the brain surface) at each location, for each ferret. After the virus injection, the craniotomy site was covered with an Amniograft membrane (in some experiments) and the removed skull. The scalp incision was closed with non-absorbable sutures and the wound site was covered with Neosporin. Animals were returned to the cage with the rest of the litter after they were ambulatory. Analgesics and antibiotics were administered through 48 hours after surgery.

Construction of ProjectorScope 2.

The ProjectorScope 2 (Fig. 1D, Supplementary Fig. 1,2) was built with several modifications of ProjectorScope 1 (Roy et al., 2016) to achieve wide patterned optogenetic stimulation and intrinsic signal imaging. Patterned light for optogenetic stimulation was generated by an LCD projector (NP3250W, NEC) and transmitted onto the brain surface by three single-lens reflex (SLR) lenses of the same type (Nikon, focal length 50 mm, f/1.2). The original projection lens was replaced with one of these SLR lenses to reduce misalignment between the projector and the rest of the optical system. Two juxtaposed lenses (L1; Thorlabs achromat, focal length 30mm, diameter 25mm) were used to minify the projection image to the appropriate size, 3mm by 3mm, in order to cover the exposed area in ferret V1. A dichroic mirror (DM; Semrock FF483/639) reflected light between 390-460 nm to activate ChR2, while allowing green and red light to pass to the CCD camera (Dalsa camera, 1M60) for intrinsic signal imaging. Intrinsic signal imaging was performed by providing 690-nm light (halide light, Lumen Dynamics, Xcite 200DC, with a filter, Semrock FF01-675/67-25)

over the brain surface and taking images of the reflected light using the CCD, with an SLR lens (Nikon, focal length 135 mm, f/2.8) to bring the image into focus. The maximum power that the system can provide is approximately 10mW/mm2 measured at 475 nm by projecting a full-field, 100% contrast white image. ProjectorScope 2 allows three-dimensional adjustments for easier focus on a curved brain surface (details seen in Supplementary Fig. 1,2).

Non-survival surgery.

About 4 weeks after the virus injection, the ferrets were sedated with ketamine (20mg/kg, IM). Atropine (0.16mg/kg, IM) and dexamethasone (0.5mg/kg, IM) were administered to reduce bronchial and salivary secretion and to reduce inflammation, respectively. The animal was anesthetized with a mixture of isoflurane, oxygen, and nitrous oxide through a mask while a tracheostomy was performed. Animals were then ventilated with 1.5%–3% isoflurane in a 2:1 mixture of nitrous oxide and oxygen. A cannula was inserted into the intraperitoneal cavity for delivery of neuromuscular blockers and Ringer's solution (3 ml/kg/hr), and the animal was placed in a custom stereotaxic frame that did not obstruct vision. The head was fixed with a custom head plate that allowed pitch adjustments for imaging. All wound margins were infused with bupivacaine. Silicone oil was placed on the eyes to prevent corneal drying. A craniotomy (4 by 4mm) was made in the right hemisphere centered around the virus injection site, and the dura was removed with a 31-gauge needle. A few drops of liquid agarose were applied on the exposed brain surface, and, while the agarose was still liquid, a pre-drilled coverslip (a hole of about 700um in diameter was drilled through the coverslip) was mounted on top of the craniotomy area and held until the agarose became solid (Levy et al., 2012). The coverslip edge was secured using cyanoacrylate glue and excess agarose on the coverslip was removed. Next, the ferrets were paralyzed with the neuromuscular blocker gallamine triethiodide (10–30 mg/kg/hr) through the intraperitoneal cannula to suppress spontaneous eye movements, and the nitrous oxide-oxygen mixture was adjusted to 1:1. The animal's ECG was continuously monitored to ensure adequate anesthesia, and the percentage of isoflurane was increased if the ECG indicated any distress. Body temperature was maintained at 37°C.

Visual stimulation.

Visual stimuli were created in MATLAB with the Psychophysics Toolbox on a Macintosh Pro running OSX and displayed on a Sony monitor (GDM-520). The monitor was placed 35cm in front of the ferret. Stimuli were full field sine wave gratings with 0.15 spatial frequency and 4Hz temporal frequency.

For intrinsic signal imaging experiments, 100% contrast, bidirectional grating stimuli with orientations varied from 0° to 135° with a step of 45° were played. Each orientation condition was repeated 20 times with 10s inter-stimulus-interval and 5s stimulus duration.

For the optogenetic experiments, visual stimuli were 100% contrast, full-field, with 0.15 spatial frequency, 4Hz temporal frequency with 8 cycles and repeated 5 times with 3-5s inter-stimulus-interval. To measure the orientation selectivity, the orientations were varied from 0° to 157.5° with a step of 22.5°. To measure responses to visual contrast, the orientation was fixed at the preferred angle and the contrasts were varied as 16%, 32%, 64%, or 100%.

Intrinsic signal imaging. Intrinsic signal imaging was performed for some optogenetic experiments to obtain the orientation column maps. With ProjectorScope 2, 690-nm light illuminated the brain surface and the reflected light from the brain surface was captured by the camera. The images were acquired at 30 Hz with custom software in LabVIEW and a National Instruments PCI-1426 acquisition board. The raw images were averaged for every 0.5s and the image that was 0.5s before the onset of the stimulus was used as the baseline image. The single condition images representing responses for individual orientations were averaged over all repetitions and the orientation column map was generated by calculating the vector summation of responses in the single condi-

tion images:

$$P = \sum_{k=1}^{N} R(\theta_k) e^{\frac{2\pi i \theta_k}{180^\circ}} \quad (1)$$

where $R(\theta_k)$ is the responses in a single condition image for a certain orientation stimulus, and P represents the response of each pixel in the map as a vector summation in the complex plane.

Electrophysiology.

In some optogenetic experiments and optogenetic specificity experiments, single barrel carbon fiber electrodes were used (E1011, Kation Scientific). Such carbon fiber electrodes have very small tips of about 5um in diameter so they minimize damage to the brain tissue and do not cast shadows over the stimulated brain area. One electrode was inserted through the hole on the coverslip into ferret V1, and was lowered to a depth that ranged from 100um to 400um below the brain surface. The signals were amplified by RHD2132 and collected by the RHD2000 evaluation board (Intan Technologies).

In the inhibitory optogenetic experiments, a custom 32-channel probe (S-probe, Plexon) was used. Instead of using pre-drilled coverslips, the probe was positioned to just touch the brain surface and 2

Optogenetic receptive zone.

We characterized the optogenetic receptive zone (ORZ) for each patterned optogenetic experiment. To measure the spatial range of the effective optogenetic stimulation, we projected small dots, 750um in diameter, in a randomized fashion tiling across the entire projection area, 3 by 3 mm2, onto the ferret primary visual cortex that had ChR2 expression. We determined whether a cell's response at any of the stimulus positions was significantly different from the response to a "blank" stimulus by performing an ANOVA test (P<0.05). Responses were fitted by a bivariate Gaussian function to estimate the region over which a cell was strongly activated :

$$R(s) = NR\left\{\left[\sum_x \sum_y G(x, y, \mu, \Sigma) I_s(x, y)\right], a, c_{50}, n\right\} \quad (2)$$

Where $I_s(x, y)$ is the intensity at point x,y for stimulus s, $G(x, y, \mu, \Sigma)$ is the bivariate Gaussian with mean μ and covariance matrix Σ, and $NR(c, a, c_{50}, n)$ is the Naka-Rushton function:

$$NR(c, a, c_5 0, n) = \frac{ac^n}{c^n + (c_{50})^n} \quad (3)$$

Where a is the maximum cell response, c is the stimulus intensity, and c_{50} is the intensity of a stimulus that produces half of the maximum response. Variables a, c_{50}, n, μ, Σ were used as free parameters for the fit. The size of the ORZ was taken to be the full width at half-height (FWHH) along the major and minor axes of $G(x, y, \mu, \Sigma)$.

Patterned optogenetic stimulation.

In patterned optogenetic specificity experiments, stimulation masks targeting specific orientation columns were generated based on the map acquired during intrinsic signal imaging (custom software, MATLAB). The preferred orientation of the recorded neuron was identified as the orientation that evoked the strongest visual responses from the orientation tuning curve. Visual contrast tuning curves were initially measured using 16%, 32%, 64%, or 100% contrast. The optogenetic light intensity tuning curve were measured by projecting the mask of the ORZ with varying image intensities, 20%, 40%, 60%, 80%. The measurements of these tuning curves were repeated by changing contrasts or intensities until comparable levels between visual and optogenetic responses were found, which was usually achieved after 2-3 iterations. Five levels of visual contrasts or light intensities, including 0% contrast and 0% intensity, were chosen for each cell. For the combined visual and patterned optogenetic stimulation, each visual stimulus was paired with an optogenetic mask

stimulus and each pair started at the same time with the optogenetic stimulation lasting for 1s and visual stimulation lasting for 2s. The orientation column masks for a given angle were made by including all pixels in the intrinsic signal imaging map that matched the specified angle within some tolerance. The tolerance (or thickness) of the column masks was varied by changing the range of orientation angles that each column mask contained: 15°, 30°, or 45° tolerance. We found that a tolerance of 15° was too small for some cells to evoke enough optogenetic responses and that a tolerance of 45° was too big to create distinctly complementary patterns of inputs, so, in the analysis here, we only report the results based on 30° masks. The stimulation order was randomized.
For all-optogenetic stimulation (Fig. 3A), the masks were created to target either the preferred orientation columns that were revealed in the orientation columns map, the orthogonal orientation columns, or both. For hybrid stimulation (Fig. 3B), the masks were created to target the orthogonal orientation columns and the visual stimulus presented the preferred orientation. For the optogenetic specificity experiments, only the orientation columns inside the ORZ were included and the masks were created to target the orientations from 0° to 157.5° with a step of 22.5° and a tolerance of 15°.

Pharmacological blocking experiments.

To test the hypotheses of optogenetic specificity, an NMDA antagonist (DL-2-Amino-5-phosphonopentanoic acid, APV, 1mM- 5mM) and an AMPA antagonist (2,3-Dioxo-6-nitro-1,2,3,4-tetrahydrobenzo[f]quinoxaline-7-sulfonamide, NBQX, 100uM-1mM) were used to block NMDA and AMPA receptors. For these experiments, the coverslips were pre-drilled with two holes that were 2-3mm apart, one for the carbon fiber electrode and one for the blocker pipette. A pulled glass pipette similar to the dimension used in virus injections was used to apply the blockers and the blocker solution was delivered by Nanoject, with 69nl/pulse, 4 pulses/min, for 14 min, for a total volume of 3.8ul. The effectiveness of the blockers was tested by examining visual responses.

Data analysis.

Extracellular data was extracted using 4-5 standard deviations as the threshold and then clustered using K-means or KlustaKwik based on either two-point features (for the single barrel carbon fiber electrode recordings) or the principal components (for the S-probe recordings). In the patterned optogenetic experiments, the firing rates were calculated as spike counts from the 0.5s-1s after the onset of the stimuli divided by 0.5s duration, because the firing rates reached the steady states after 500ms of stimulation. In the inhibitory optogenetic experiments, the calculations of firing rates were based on the entire 1s duration of paired stimulation.
To analyze the optogenetic specificity, the specificity index is defined as 1-circular variance (Ringach et al., 2002; Mazurek et al., 2014), calculated as:

$$1 - \text{CirVar} = \frac{\sum_k R(\theta_k) e^{2i\theta_k}}{\sum_k R(\theta_k)} \tag{4}$$

Where $R(\theta_k)$ is the response to angle θ_k. The comparison between the specificity before and after blockers applications was based on two-sample t-test.
To calculate the Marginal Orthogonal Drive Angle (MODA), we created an weighted vector that described the influence of adding extra orthogonal drive to the linearity of a cell's response. We denote the response of a cell to a preferred contrast C_{pref} and orthogonal contrast C_{orth} as R(C_{pref}, C_{orth}). The linear prediction for the response of the cell is LP(C_{pref}, C_{orth})= R(C_{pref} ,0) + R(0,C_{orth}). The change in linearity was computed for each pair of presented orthogonal contrasts C^j_{orth}, C^k_{orth} (where the contrast C^k_{orth} must be greater than C^j_{orth}) as a vector

$$V(C_{\text{pref}}, C^j_{\text{orth}}, C^k_{\text{orth}}) = \begin{bmatrix} \Delta LP \\ \Delta R \end{bmatrix} = \begin{bmatrix} LP(C_{pref}, C^k_{\text{orth}}) - LP(C_{pref}, C^j_{\text{orth}}) \\ R(C_{pref}, C^k_{\text{orth}}) - R(C_{pref}, C^j_{\text{orth}}) \end{bmatrix} \tag{5}$$

To compute an accurate estimate of the Marginal Orthogonal Drive, we computed this quantity over the 2 highest preferred orientation contrasts, and for all pairs of orthogonal contrasts (there were 4 orthogonal contrasts, so there are 6 pairs of orthogonal contrasts where the second is greater than the first). Further, we normalized the contribution of each vector to the overall Marginal Orthogonal Drive by the change in orthogonal contrast, reasoning that if we added an extra amount (say, twice) of orthogonal stimulus contrast to one pair of stimuli as compared to another pair, we ought to divide the contribution by that extra amount (say, by 2) to normalize the contribution of the contrasts used, so that the vector has units of change in response per unit contrast. The total Marginal Orthogonal Drive vector was thus:

$$\vec{V} = \sum_{i=1}^{2} \sum_{j=1}^{3} \sum_{k=j+1}^{4} \frac{\vec{V}\left(C^{i}_{\text{pref}}, C^{j}_{\text{orth}}, C^{k}_{\text{orth}}\right)}{C^{k}_{\text{orth}} - C^{j}_{\text{orth}}} \tag{6}$$

where i represents the two highest contrasts of the preferred stimulus, and j and k represent the levels of orthogonal contrast from which the starting data point and the ending data point of a vector are found.

The Marginal Orthogonal Drive Length is then

$$\text{MODL} = \sqrt{V[1]^2 + V[2]^2 +} \tag{7}$$

and the Marginal Orthogonal Drive Angle is

$$\text{MODA} = \tan^{-1}\left(\frac{V[2]}{V[1]}\right) \tag{8}$$

where $V[i]$ is the ith dimension of the vector V.

The Linearity index is the slope of the best linear fit line of R and LP (in the least squares sense) that passes through all responses under all contrasts and must pass through the origin.

Ring model simulations.

The ring models consisted of 180 E and I cells, placed along a ring. Each position was given a label θ_i = 0…179°. The steady-state response of each cell was given by the equation from Rubin et al. 2015:

$$r_i^{ss} = 0.04\left[\sum_{j=1}^{N} w_{ij} r_j + h_i\right]_+^2 \tag{9}$$

where w_{ij} is the connection from neuron j to neuron i, and hi is the sum of visual (hvisual) and optogenetic (hopto) input to neuron i. The connections from e-to-e neurons had a weight W_{EE} that fell off in a Gaussian manner with angular distance around the ring as σ_{EE}. Similarly, connections from i-to-e had a value W_{EI} that fell off with σ_{EI}, connections from e-to-i had a value W_{IE} that fell off with σ_{IE}, and i-to-i connections had a weight W_{II} that fell off with σ_{II}. The following differential equation was solved numerically using Euler's method:

$$\tau_i \frac{dr_i}{dt} = -r_i + r_i^{ss} \tag{10}$$

where τ_i is 200ms for excitatory cells and 100ms for inhibitory cells. Visual stimulation at an angle θ was delivered to each neuron with a strength of 1 and a Gaussian falloff of 30°.

The details of the connections and optogenetic input differed by model. For Model 1, W_{EE} was 0.018, W_{EI} was -0.0094, W_{IE} was 0.0171, W_{II} was -0.0073, and σ_{EE} = σ_{IE} = σ_{EI} = σ_{II} = 32°. Optogenetic input was delivered to each neuron with a strength of 1 and a Gaussian falloff of 45° from the angle of columnar stimulation θ.

For Model 2, the parameters were the same as Model 1, except that visual and optogenetic inputs to inhibitory neurons were slightly increased (to 1.1), and σ_{EE} = σ_{IE} = σ_{II} = 10°, while σ_{EI} was dropped to 25°

For Model 3, the parameters were the same as Model 2, except that optogenetic input was modeled differently. The orthogonal input was modeled as the sum of $\frac{1}{2}$ the Gaussian fall off as before and a constant input of 0.5 at all θ_i, and the preferred input included an additional 0.2 input to inhibitory neurons to reflect the fact that the preferred optogenetic stimulation included the region right around the electrode (which was omitted in the orthogonal input). That is, the input to excitatory neurons was given as the real part of the following equations, and the input to inhibitory neurons was given as the imaginary part of the following equations:

$$h_{\text{opto}}^{\text{orth}} = (1 + 1.1i)(0.5G(1, 45\text{-}) + 0.5) \tag{11}$$

$$h_{\text{opto}}^{\text{pref}} = (1 + 1.1i)(0.5G(1, 45\text{-}) + 0.5) + 0.2i \tag{12}$$

Heterogeneous network simulations.

To simulate the impact of optogenetic stimulation in a heterogeneous network with variable optogenetic activation and variable synaptic weights, we simulated a column with 2 populations with N neurons in it, each with steady-state rate $\vec{r}$ given by:

$$\vec{r} = \phi\left(W\vec{r} + \vec{h}\right) \tag{13}$$

Where the function ϕ is a modified rectified power law function $\phi(x) = (\alpha x)^n/(1 + (x + \alpha)^n)$, which saturates for $x \to \infty$ and behaves similarly to the standard rectified power law or small values of x. We chose alpha =35 and $n = 2$ The connectivity elements are sparse with sparsity $p = 0.3$. The nonzero elements of W are w_{ee}=1, w_{ei}=1.1, w_{ie}=0.89, w_{ii}=0.91 and they scale as 1/N with the network size.

The external inputs to each neuron h_i^α have a baseline component and an optogenetic input, such that

$$h_i^\alpha = h_i^{\text{b},\alpha} + I_i^{\text{Chr2}}(x)\delta_{\alpha I} \tag{14}$$

The baseline was uniformly distributed $h^{\text{b},\alpha}$, centered in $\mu_{h^{\text{b}}} = 10$ and with a width $\sigma_{h^{\text{b}}} = 6$ for both cell types. The optogenetic input only affects inhibitory neurons and is defined below.

Model of Optogenetic Perturbations

There were two main sources of photocurrent heterogeneity, one being light dispersion through the tissue and the second one being the number or ChR2 channels that are expressed in each cell. Regarding the first one the amount of light that reaches the cells decays exponentially with distance (Yona et. al. 2016). We assumed that the recorded neurons are homogeneously distributed in the z axis of the probe. The light that arrived to each neuron was given by

$$l_i(x) = 2x \exp\left(\frac{-z_i}{\lambda}\right) \qquad \text{with} \qquad z_i \sim U(0, 1) \tag{15}$$

Where x is the light intensity at the surface, z_i is the distance of the cell i from the surface, and λ is the spatial scale (We took $\lambda = 2$). We assumed that, each channel had an input output function that is given by a Hill Equation and that each channel had a different threshold, given by l_i^0

$$H_i(x) = \frac{(l_i(x) - l_i^0)^\gamma}{1 + (l_i(x) - l_i^0)^\gamma} \tag{16}$$

With $l_i^0 = l_i(x_0)$, with $x_0 \sim \mathcal{N}(\mu_{x_0}, \sigma_{x_0})$. The values were chosen to be $\mu_{x_0} = -0.05$ while $\sigma_{x_0} = 0.001$. The second source of heterogeneity is the number of ChR2 channels that are expressed with the virus, that we assume to be gaussian distributed. In the simulations, we didn't specify the number of channels, but we used a normalized number distributed as $\kappa c \sim \mathcal{N}(\mu_c, \sigma_c)$ with $\mu_c = 72$ and $\sigma_c = 8$

Each individual channel contributed independently and identically to the photocurrent such that the total input to the cell was

$$I_i^{\text{Chr2}}(x) = \kappa c_i (H_i(x) - H_i(0)) \tag{17}$$

Where the substraction by $H_i(0)$ guaranteed that the effect of the laser at zero intensity (x=0) was 0.

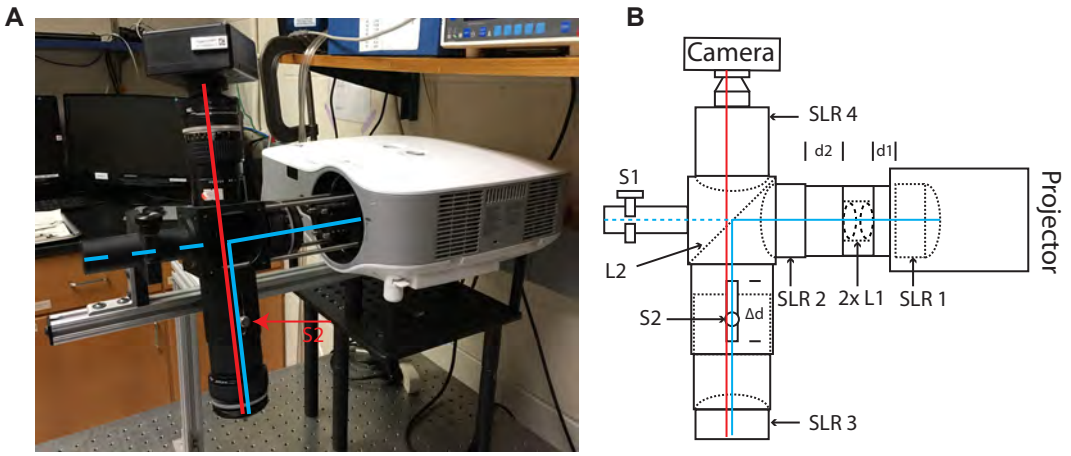

Figure S1. ProjectorScope 2. ProjectorScope 2 on the experimental table. The blue axis represents the direction of the outgoing light from the projector reflected by a dichroic mirror. The red axis represents the direction along which light travels from the brain surface to the camera during intrinsic signal imaging. The red arrow points to the tube that provides translation along the red axis using set screw S2. **B.** A schematic of ProjectorScope 2. SLR, single-reflex lens; S1, screw 1; S2, screw 2; 2x L1, two closely placed achromat lenses; L2, dichroic mirror; d1=30mm; d2=45mm; Δd = 6cm.

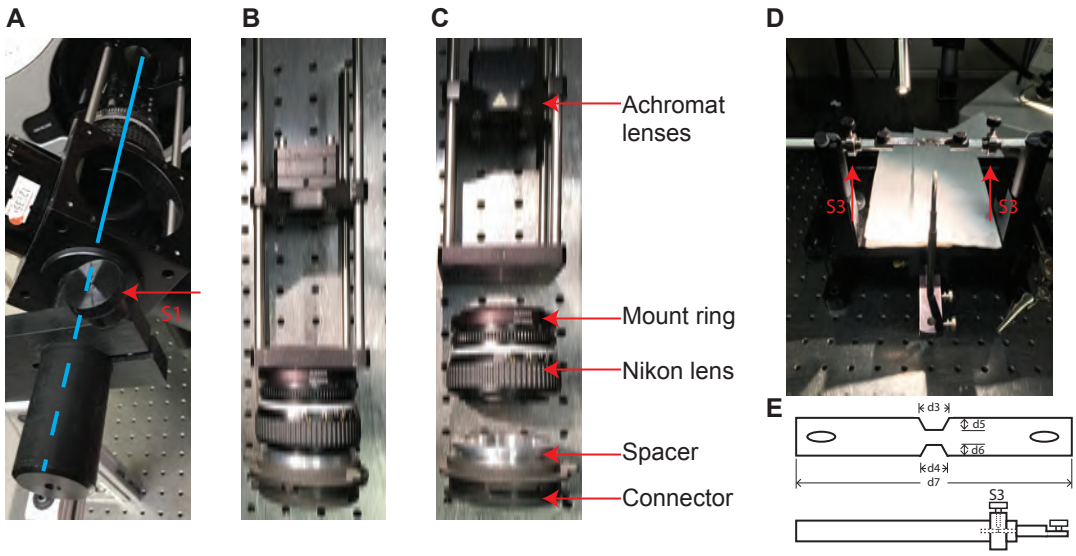

Figure S2. Components of ProjectorScope 2 and the custom head-plate and head-bars. A. The cylindrical bar that allows the cube to rotate around the blue axis. The knob S1 controls the rotation of the bar. **B.** The replaced projection lens with all components connected. **C.** A disconnected version of B, which separately displays the connector to the projector, the spacer, the Nikon lens, and the custom-made mount ring that connects the Nikon lens to the Thorlabs rectangular connector. **D.** The rotatable headplate. The red arrows point to the rotatable parts, S3, that can adjust the animal's head pitch angle. Combing the controllable parts in S1, S2, and S3, ProjectorScope 2 allows three-dimensional adjustments for easier focus on a curved brain surface. **E.** Schematics of the head-plate and the head-bar. The head-plate, 1mm thick, has two half-hexagon notches to easily fit the curved skull surface. d3=7mm, d5=2mm, d4=5mm, d6=1.5mm, d7=6.5cm. The head-bar provides rotation by adjusting S3.

Supplementary Figure 8-1

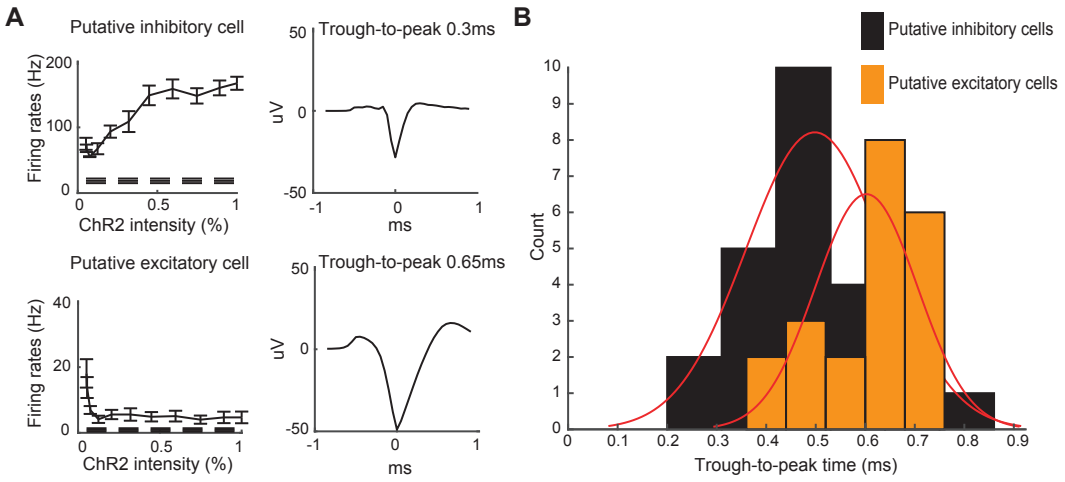

Figure S3. Optogenetic stimulation of ferrets expressing mDlx-ChR2 revealed neurons with putative excitatory and inhibitory signatures. A. Left) Responses of an example putative inhibitory cell (top) that shows direct activation by light stimulation, and a putative excitatory cell (bottom) that is strongly inhibited by light. Raw responses are shown, without visual stimulation, and without any subtraction of background firing rates (dashed line). Right) Zoomed-in views of the average action potential waveform from each neuron along with the trough-to-peak time. **B.** Histograms of trough-to-peak times of putative inhibitory cells and putative excitatory cells. Cells' identities were first determined by their response profiles to optogenetic stimulation and then the trough-to-peak times were calculated and summarized. Gaussian density fits to the histograms are shown in red. On average, the putative excitatory cells showed longer spike durations than the inhibitory cells, although there were putative inhibitory cells that exhibited wider spikes, consistent with the variety of interneuron types found in cortex (fast-spiking and regular-spiking).

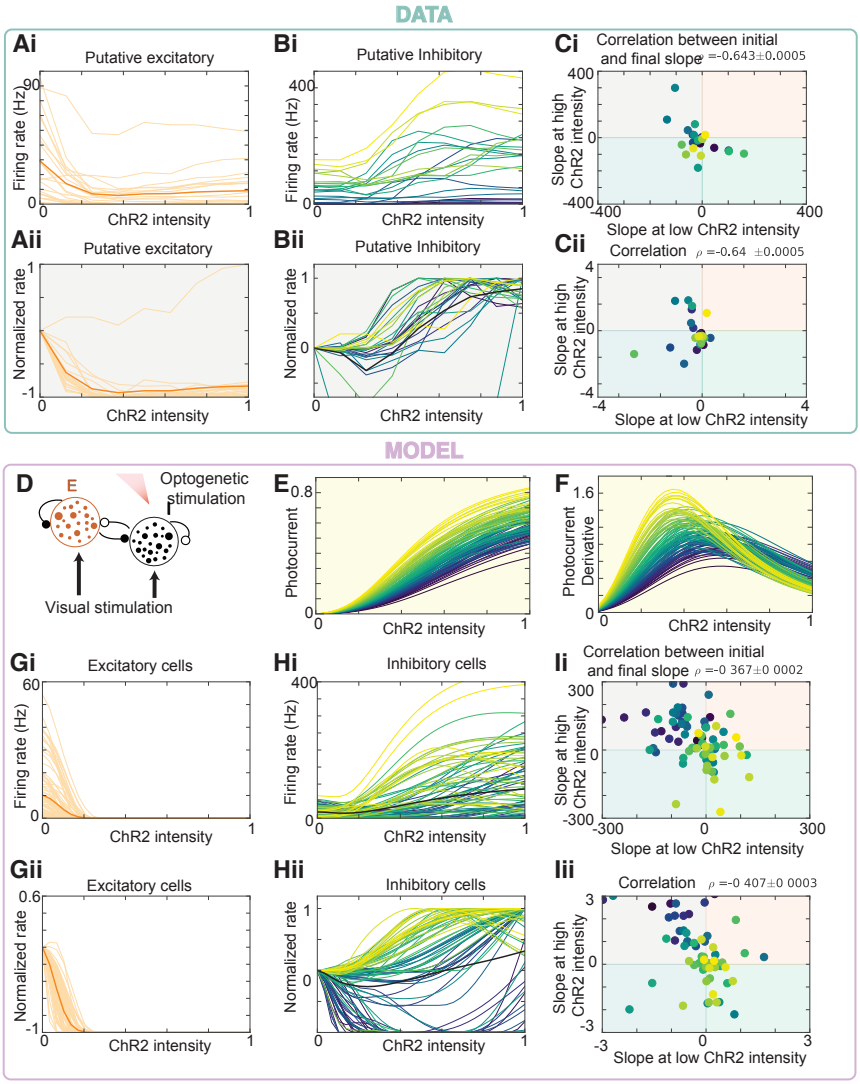

Figure S4. Optogenetic stimulation of ferrets expressing mDlx-ChR2 revealed neurons with putative excitatory and inhibitory signatures. TOP: **Ai:** Putative excitatory cells (as defined in Fig. S3.) as a function of the intensity of the optogenetic input to the inhibitory cells. **Aii:** Same as Ai but normalized such that the curves start from zero and were maximal at 1 (as in Fig. 8c). **Bi:** and **Bii:** Putative inhibitory cells. The paradoxical effect (i.e. that some cells decrease their activity upon optogenetic drive) is better revealed by normalizing the cells. **Ci:** The slope of each cells response to a weak laser input is negatively correlated with the slope at a large laser input. In other words, the cells that did not respond paradoxically tended to saturate at smaller laser intensities. **Cii:** Negative correlation for normalized responses. BOTTOM: **D:** Heterogeneous model with N neurons (N=500 in simulations). **E:** Model of optogenetic current for each cell as a function of laser intensity as given by Eq. 17. **F:** Derivative of the photocurrent. **Gi:** Excitatory cells as a function of the intensity of the optogenetic input to the inhibitory cells. **Gii:** Same as Ai but normalized such that the curves start form zero and are maximal at 1. **Hi:** and **Hii:** Inhibitory cells. The paradoxical effect in the model is better revealed by normalizing the cells, as in the data. **Ii:** and **Iii:** The model captures the negative correlation between the slope in response to a weak laser and the slope at a large laser input for both normalized and non-normalized responses.

References

1. Adelson EH, Movshon JA (1982) Phenomenal coherence of moving visual patterns. Nature 300:523-525.
2. Adesnik H (2017) Synaptic Mechanisms of Feature Coding in the Visual Cortex of Awake Mice. Neuron 95:1147-1159 e1144.
3. Ahmadian Y, Rubin DB, Miller KD (2013) Analysis of the stabilized supralinear network. Neural Comput 25:1994-2037.
4. Anderson JS, Carandini M, Ferster D (2000) Orientation tuning of input conductance, excitation, and inhibition in cat primary visual cortex. J Neurophysiol 84:909-926.
5. Anderson JS, Lampl I, Gillespie DC, Ferster D (2001) Membrane potential and conductance changes underlying length tuning of cells in cat primary visual cortex. J Neurosci 21:2104-2112.
6. Asrican, Brent, et al. "Next-generation transgenic mice for optogenetic analysis of neural circuits." Frontiers in neural circuits 7 (2013): 160.
7. Baker CA, Elyada YM, Parra A, Bolton MM (2016) Cellular resolution circuit mapping with temporal-focused excitation of soma-targeted channelrhodopsin. eLife 5.
8. Berndt A, Schoenenberger P, Mattis J, Tye KM, Deisseroth K, Hegemann P, Oertner TG (2011) High-efficiency channelrhodopsins for fast neuronal stimulation at low light levels. Proc Natl Acad Sci U S A 108:7595-7600.
9. Bishop PO, Coombs JS, Henry, H. G (1973) Receptive fields of simple cells in the cat striate cortex. J Physiol 231:31-60.
10. Blasdel GG, Salama G (1986) Voltage-sensitive dyes reveal a modular organization in monkey striate cortex. Nature 321:579-585.
11. Bonds AB (1989) Role of inhibition in the specification of orientation selectivity of cells in the cat striate cortex. Vis Neurosci 2:41-55.
12. Boyden ES, Zhang F, Bamberg E, Nagel G, Deisseroth K (2005) Millisecond-timescale, genetically targeted optical control of neural activity. Nat Neurosci 8:1263-1268.
13. Busse L, Wade AR, Carandini M (2009) Representation of concurrent stimuli by population activity in visual cortex. Neuron 64:931-942.
14. Carandini M, Heeger DJ (2011) Normalization as a canonical neural computation. Nat Rev Neurosci 13:51-62.
15. Carandini M, Heeger DJ, Movshon JA (1997) Linearity and Normalization in Simple Cells of the Macaque Primary visual Cortex. J Neurosci 17:8621-8644.
16. Cardin JA, Palmer LA, Contreras D (2007) Stimulus feature selectivity in excitatory and inhibitory neurons in primary visual cortex. J Neurosci 27:10333-10344.
17. Cavanaugh JR, Bair W, Movshon JA (2002) Nature and interaction of signals from the receptive field center and surround in macaque V1 neurons. J Neurophysiol 88:2530-2546.
18. Chisum HJ, Mooser F, Fitzpatrick D (2003) Emergent properties of layer 2/3 neurons reflect the collinear arrangement of horizontal connections in tree shrew visual cortex. J Neurosci 23:2947-2960.
19. Das A, Gilbert CD (1999) Topography of contextual modulations mediated by short-range interactions in primary visual cortex. Nature 399:655-661.
20. DeAngelis GC, Robson JG, Ohzawa I, Freeman RD (1992) Organization of suppression in receptive fields of neurons in cat visual cortex. J Neurophysiol 68:144-163.
21. Dimidschstein J et al. (2016) A viral strategy for targeting and manipulating interneurons across vertebrate species. Nat Neurosci 19:1743-1749.
22. Freeman TC, Durand S, Kiper DC, Carandini M (2002) Suppression without inhibition in visual cortex. Neuron 35:759-771.
23. Grinvald A, Lieke E, Frostig RD, Gilbert CD, Wiesel TN (1986) Functional architecture of cortex revealed by optical imaging of intrinsic signals. Nature 324:361-364.

24. Haider B, Krause MR, Duque A, Yu Y, Touryan J, Mazer JA, McCormick DA (2010) Synaptic and network mechanisms of sparse and reliable visual cortical activity during nonclassical receptive field stimulation. Neuron 65:107-121.
25. Heeger DJ (1992) Normalization of cell responses in cat striate cortex. Vis Neurosci 9:181-198.
26. Heuer HW, Britten KH (2002) Contrast dependence of response normalization in area MT of the rhesus macaque. J Neurophysiol 88:3398-3408.
27. Hirsch JA, Martinez LM, Pillai C, Alonso JM, Wang Q, Sommer FT (2003) Functionally distinct inhibitory neurons at the first stage of visual cortical processing. Nat Neurosci 6:1300-1308.
28. Histed MH (2018) Feedforward Inhibition Allows Input Summation to Vary in Recurrent Cortical Networks. eNeuro 5.
29. Huang X, Elyada YM, Bosking WH, Walker T, Fitzpatrick D (2014) Optogenetic assessment of horizontal interactions in primary visual cortex. J Neurosci 34:4976-4990.
30. Katzner S, Busse L, Carandini M (2011) GABAA inhibition controls response gain in visual cortex. J Neurosci 31:5931-5941.
31. Kerlin AM, Andermann ML, Berezovskii VK, Reid RC (2010) Broadly tuned response properties of diverse inhibitory neuron subtypes in mouse visual cortex. Neuron 67:858-871.
32. Lauritzen TZ, Krukowski AE, Miller KD (2001) Local correlation-based circuitry can account for responses to multi-grating stimuli in a model of cat V1. J Neurophysiol 86:1803-1815.
33. Levy M, Schramm AE, Kara P (2012) Strategies for mapping synaptic inputs on dendrites in vivo by combining two-photon microscopy, sharp intracellular recording, and pharmacology. Front Neural Circuits 6:101.
34. Li B, Thompson JK, Duong T, Peterson MR, Freeman RD (2006) Origins of cross-orientation suppression in the visual cortex. J Neurophysiol 96:1755-1764.
35. Litwin-Kumar A, Rosenbaum R, Doiron B (2016) Inhibitory stabilization and visual coding in cortical circuits with multiple interneuron subtypes. J Neurophysiol 115:1399-1409.
36. Liu BH, Li P, Li YT, Sun YJ, Yanagawa Y, Obata K, Zhang LI, Tao HW (2009) Visual receptive field structure of cortical inhibitory neurons revealed by two-photon imaging guided recording. J Neurosci 29:10520-10532.
37. MacEvoy SP, Tucker TR, Fitzpatrick D (2009) A precise form of divisive suppression supports population coding in the primary visual cortex. Nat Neurosci 12:637-645.
38. Mahrach A, Chen G, Li N, van Vreeswijk C, Hansel D (2020) Mechanisms underlying the response of mouse cortical networks to optogenetic manipulation. eLife 9.
39. Mazurek M, Kager M, Van Hooser SD (2014) Robust quantification of orientation selectivity and direction selectivity. Front Neural Circuits 8:92.
40. Mehta P, Kreeger L, Wylie DC, Pattadkal JJ, Lusignan T, Davis MJ, Turi GF, Li WK, Whitmire MP, Chen Y, Kajs BL, Seidemann E, Priebe NJ, Losonczy A, Zemelman BV (2019) Functional Access to Neuron Subclasses in Rodent and Primate Forebrain. Cell Rep 26:2818-2832 e2818.
41. Morrone MC, Burr DC, Maffei L (1982) Functional implications of cross-orientation inhibition of cortical visual cells. I. Neurophysiological evidence. Proc R Soc Lond B 216:335-354.
42. Morrone MC, Burr DC, Speed HD (1987) Cross-orientation inhibition in cat is GABA mediated. Exp1 Brain Res 67:635-644.
43. Nassi JJ, Avery MC, Cetin AH, Roe AW, Reynolds JH (2015) Optogenetic Activation of Normalization in Alert Macaque Visual Cortex. Neuron 86:1504-1517.
44. Niell CM, Stryker MP (2008) Highly selective receptive fields in mouse visual cortex. J Neurosci 28:7520-7536.
45. Ozeki H, Finn IM, Schaffer ES, Miller KD, Ferster D (2009) Inhibitory stabilization of the cortical network underlies visual surround suppression. Neuron 62:578-592.
46. Palmigiano A, Fumarola F, Mossing DP, Kraynyukova N, Adesnik H, Miller KD (2020) Structure and variability of optogenetic responses identify the operating regime of cortex. bioRxiv:2020.2011.201
47. Popovic M, Stacy AK, Kang M, Nanu R, Oettgen CE, Wise DL, Fiser J, Van Hooser SD (2018) Development of Cross-Orientation Suppression and Size Tuning and the Role of Experience.

J Neurosci 38:2656-2670.

48. Priebe NJ (2016) Mechanisms of Orientation Selectivity in the Primary Visual Cortex. Annu Rev Vis Sci 2:85-107.
49. Priebe NJ, Ferster D (2006) Mechanisms underlying cross-orientation suppression in cat visual cortex. Nat Neurosci 9:552-561.
50. Reynolds JH, Heeger DJ (2009) The normalization model of attention. Neuron 61:168-185.
51. Ringach DL, Shapley RM, Hawken MJ (2002) Orientation selectivity in macaque V1: diversity and laminar dependence. J Neurosci 22:5639-5651.
52. Rochefort NL, Garaschuk O, Milos RI, Narushima M, Marandi N, Pichler B, Kovalchuk Y, Konnerth A (2009) Sparsification of neuronal activity in the visual cortex at eye-opening. Proc Natl Acad Sci U S A 106:15049-15054.
53. Roy A, Osik JJ, Ritter NJ, Wang S, Shaw JT, Fiser J, Van Hooser SD (2016) Optogenetic spatial and temporal control of cortical circuits on a columnar scale. J Neurophysiol 115:1043-1062.
54. Rubin DB, Van Hooser SD, Miller KD (2015) The stabilized supralinear network: a unifying circuit motif underlying multi-input integration in sensory cortex. Neuron 85:402-417.
55. Saleem AB, Diamanti EM, Fournier J, Harris KD, Carandini M (2018) Coherent encoding of subjective spatial position in visual cortex and hippocampus. Nature 562:124-127.
56. Sanzeni A, Akitake B, Goldbach HC, Leedy CE, Brunel N, Histed MH (2020) Inhibition stabilization is a widespread property of cortical networks. eLife 9.
57. Sato TK, Hausser M, Carandini M (2014) Distal connectivity causes summation and division across mouse visual cortex. Nat Neurosci 17:30-32.
58. Sato TK, Haider B, Hausser M, Carandini M (2016) An excitatory basis for divisive normalization in visual cortex. Nat Neurosci 19:568-570.
59. Shushruth S, Mangapathy P, Ichida JM, Bressloff PC, Schwabe L, Angelucci A (2012) Strong recurrent networks compute the orientation tuning of surround modulation in the primate primary visual cortex. J Neurosci 32:308-321.
60. Simoncelli EP, Heeger DJ (1998) A model of neuronal responses in visual area MT. Vision Res 38:743-761.
61. Smith GB, Sederberg A, Elyada YM, Van Hooser SD, Kaschube M, Fitzpatrick D (2015) The development of cortical circuits for motion discrimination. Nat Neurosci 18:252-261.
62. Smith MA, Bair W, Movshon JA (2006) Dynamics of suppression in macaque primary visual cortex. J Neurosci 26:4826-4834.
63. Sohya K, Kameyama K, Yanagawa Y, Obata K, Tsumoto T (2007) GABAergic neurons are less selective to stimulus orientation than excitatory neurons in layer II/III of visual cortex, as revealed by in vivo functional Ca2+ imaging in transgenic mice. J Neurosci 27:2145-2149.
64. Suarez H, Koch C, Douglas R (1995) Modeling direction selectivity of simple cells in striate visual cortex within the framework of the canonical microcircuit. J Neurosci 15:6700-6719.
65. Tsodyks MV, Skaggs WE, Sejnowski TJ, McNaughton BL (1997) Paradoxical effects of external modulation of inhibitory interneurons. J Neurosci 17:4382-4388.
66. Vormstein-Schneider D et al. (2020) Viral manipulation of functionally distinct interneurons in mice, non-human primates and humans. Nat Neurosci 23:1629-1636.
67. Wilson DE, Smith GB, Jacob AL, Walker T, Dimidschstein J, Fishell G, Fitzpatrick D (2017) GABAergic Neurons in Ferret Visual Cortex Participate in Functionally Specific Networks. Neuron 93:1058-1065 e1054.
68. Yona, G., Meitav, N., Kahn, I. & Shoham, S. Realistic numerical and analytical modeling of light scattering in brain tissue for optogenetic applications. eNeuro 3, 420–424 (2016).